Probabilistic Cellular Automata modeling of intercellular interactions in airways : complex pattern formation in patients with Chronic Obstructive Pulmonary Disease

Isabelle Dupin, Edmée Eyraud, Élise Maurat, Jean-Marc Sac-Épée, Pierre Vallois

Probabilistic Cellular Automata modeling of intercellular interactions in airways : complex pattern formation in patients with Chronic Obstructive Pulmonary Disease

Isabelle Dupin[1,2], Edmée Eyraud[1,2], Élise Maurat[1,2], Jean-Marc Sac-Épée[3] and Pierre Vallois[3]*

[1] Univ-Bordeaux, Centre de Recherche Cardio-thoracique de Bordeaux, U1045, F-33000 Bordeaux, France

[2] INSERM, Centre de Recherche Cardio-thoracique de Bordeaux, U1045, F-33000 Bordeaux, France

[3] Université de Lorraine, CNRS, Inria, IECL. F-54000 Nancy, France

*Email corresponding author : isabelle.dupin@u-bordeaux.fr)

Highlights

- Probabilistic Cellular Automata models fibrocytes and CD8+ T cells interplay.
- The parameters are estimated accurately from theoretical analysis and experiments.
- The dynamics of cell populations is simulated within lungs over 20 years.
- Two distinct patterns emerge, corresponding to the healthy and COPD situations.

Abstract
The chronic obstructive pulmonary disease (COPD) is a highly prevalent lung disease, in which unusual interactions between fibrocytes and CD8+ T lymphocytes in the peribronchial area could induce chronic inflammation and tissue remodeling. We considered a probabilistic cellular automata type model where the two types of cells follow simple local interaction rules taking into account cell death, proliferation, migration and infiltration. A rigorous mathematical analysis carried out within the framework of a streamlined model makes it possible to estimate with precision the parameters of the model using multiscale experimental data obtained in control and disease conditions. The simulation of the model is simple to be implemented. In simulations, two distinct patterns emerged, which can be analyzed quantitatively. In particular, we show that the change in fibrocyte density in the COPD condition is mainly the consequence of their infiltration into the lung during exacerbations, suggesting possible explanations for experimental observations in normal and COPD tissue. Our integrated approach combining probabilistic cellular automata type model and experimental findings will provide further insights into COPD in future studies.

Keywords :
Fibrocytes, lymphocytes, chronic respiratory disease, local environment, Markov process, chronic inflammation.

Fundings
This study was supported by a grant from the “Fondation Bordeaux Université”, with funding from "Assistance Ventilatoire à Domicile" (AVAD) and "Fédération Girondine de Lutte contre les Maladies Respiratoires" (FGLMR).

Declaration of interest ID have a patent (EP N°3050574 : Use of plerixafor for treating and/or preventing acute exacerbations of chronic obstructive pulmonary disease) granted. All other authors declare they have no competing interests.

1 Introduction

Chronic Obstructive Pulmonary Disease (COPD) is a chronic respiratory disease that affects adults over 40 years of age. The major risk factor is exposure to aerosolized pollutants, such as cigarette smoke. Patients with COPD often experience "exacerbations", which are periods of acute worsening of their respiratory symptoms. Exacerbations play an important role in the progression of the disease. COPD is characterized by chronic bronchial inflammation of the airways and parenchyma.

Changes in the structure of the tissue are also observed, such as lamina propria fibrosis of the so-called "distal" bronchi, i.e. bronchi with a lumen diameter of less than 2 mm, leading to persistent airflow obstruction ([20]). The understanding of the pathophysiological mechanisms of COPD has progressed thanks to animal models ([11]), in vitro studies ([23]), and expression analyses using bulk human lung tissue ([24]) and more recently at the single cell level ([2]). However, detailed knowledge of the crosstalks among multiple lung cell types and particularly their evolution along COPD development is still lacking, and treatments for COPD have seen minimal advances over the past decades ([52]).

The bronchial wall is a complex structure, and comprises different cell types, including both structural cells, such as fibrocytes and fibroblasts, and immune cells, such as lymphocytes and dendritic cells. These non-epithelial cells are sparse and they embedded in an extracellular matrix, which maintains the three-dimensional architecture of the lung by interconnecting cells, that do not adhere tightly to each other ([22]). Bronchi of COPD patients are infiltrated with a large amount of lymphocytes, and in particular CD8+ T cells. The density of CD8+ T cells in lung parenchyma and small airways inversely correlates with lung function, ([37]), suggesting the implication of CD8+ T cells in deleterious COPD evolution. On the other hand, we have previously shown in [6] that fibrocytes, circulating cells with fibroblastic properties, were present in increased levels in the blood of COPD patients at the time of an exacerbation and increased densities in the bronchi of COPD patients ([7]).

The deregulation of interactions between immune (including CD8+ T cells) and non-immune (including fibrocytes) cells could be a hallmark of chronic inflammation and tissue remodelling. In particular, it was recently shown that fibrocytes could interact with CD8+ T cells and promote their proliferation ([1]), suggesting that the interplay between these two cell types could play a role in COPD onset and evolution.

Nevertheless, we are very far from understanding how the system works at the population and tissue levels. Moreover, it is also difficult to know how the disease disrupts this system. Our working hypothesis is the following : modifications of the local interactions between fibrocytes and CD8+ T cells are the trigger to alter spatial distribution of cells, corresponding to the pathological state. This hypothesis is very difficult to test experimentally. *In vivo* progressive airflow obstruction is a complex and progressive process and an ideal model should take into account all types of cells and the associated cellular events. Therefore, we decided to build a mathematical model that only includes processes related to fibrocytes and CD8+ T cells, on which information can be drawn from experimental data.

The selected mathematical model and especially the simulations associated with it should allow to show how modifications of the local interaction rules lead to two distributions of fibrocytes and CD8+ T cells, that differ according to whether the subject considered is healthy or sick.

Two-population mathematical models include deterministic models, which classically rely on predator-prey formulation. Deterministic models are particularly pertinent to describe biological systems such as tumorsphere growth. In these models, significant insights and equations

underlying system dynamics have been partially obtained from experimental data, see for instance [3]. These models are particularly useful to describe the behaviour of the system at the population level, but do not take into account the interactions at the single cell-level. Spatial variables, critical features in our problematic to predict the tissular architecture, are usually lacking in deterministic models. This, such an approach does not sound very appropriate to model cellular crosstalk in the peri-bronchial area, where experimental data are very scarce and mostly relate to results obtained on individual-level interactions between fibrocytes and CD8+ T cells.

The individual nature of cells can be taken into account by agent-based models, which allow to derive more easily the interaction rules from experimental data. Off-lattice models, such as center-based (CBM) and deformable-cell (DCM) models, are continuous-space agent-based models that can be formulated using discrete time steps ([53], [36]) or continuous time ([38]). On-lattice models are spatially discrete models evolving in discrete time steps or in continuous time. For off-lattice as for on-lattice models, displacement of a cell is deterministic and completely defined by its velocity ([36]). Interactions between cells in off- and on-lattice models are taken into account by different types of velocity alignment. Thus, those models appear especially adapted to study the emergence of pattern formation in multicellular systems from velocity alignment interactions among cells. Among agent-based models, Lattice Gas Cellular Automaton models (see Sections 5.4 and 7 in [5]) relies on both the explicit description on agent position and its velocity. Those type of models could be relevant to our needs [16] but they are mainly used to model single and collective migration.

The framework of Probabilistic Cellular Automaton (PCA) seemed to us the most adapted to account for the local interactions of CD8+ T cells and fibrocytes. PCA are discrete-time agent-based models, in which the state of the agents evolve with time according to stochastic rules. One can find in the two monographs [5] and [30] the definition of these PCA and theoretical models. CA and PCA are widely applicable for modelling systems like forest spread ([32]), eco systems ([19]), natural patterns ([33]), neuronal networks ([42]), epidemic systems ([10]). PCA have also been used in life sciences, for example to study adult neurogenesis for teleost fishes in [28] and cell differentiation in [50]. Interestingly, previous agent-based computational approaches have been used in the field of lung science to describe the allergic inflammatory response ([39] and [40]) and airway remodelling in asthma ([44]). Thus, we decided to use PCA to model macroscopic behavior starting from microscopic interaction rules governing fibrocytes and CD8+ T cells behaviours. In contrast to "classical" PCA, which evolves synchronously in discrete time and in which the updating concerns all the cells, we have made the cells evolve one after the other as in [12] and [25]. The probability that a cell moves, dies or proliferates depends on the number of cells present in a nearby neighbourhood. We will be able to access qualitative estimates of these probabilities thanks to data from the literature and from experiments : for example, we will be able to compare the attraction/proliferation potential of CD8+ T cells purified from tissues/blood of healthy subjects or patients with COPD.

Let us briefly outline the organization of the paper. We describe in Section 2.1 the individual behavior of the CD8+ T cells and fibrocytes and their mutual dynamics is presented in Section 2.1.10. We show that our model is Markovian and ergodic in Section 2.2. We assume that for a healthy subject as for a sick subject, the same model applies, but with different parameters. We introduce in Section 2.3 a streamlined model which is obtained for some specific values of the parameters. In this setting, a rigorous mathematical analysis makes it possible to both estimate the parameters and measure the quality of these estimates (see Section 3.1).

Our model can be simulated, we present in Section 3.2 some outputs of the simulations of the streamlined model. The conclusion and discussion are found in Section 4. The proofs of technical points are postponed in Section 5.

2 Materials and methods

2.1 Model definition and notations

2.1.1 General definition

CD8+ T cells and fibrocytes are noted respectively in the following C and F.
The model takes into consideration cell displacement, death, proliferation and infiltration, that occurs at the stable state and during exacerbation. Indeed, C and F cells have a limited lifespan that depends on cell type and they can therefore be affected by cell death. When the cells are alive, C cells can move and proliferate, whereas F can only move (see Section 2.1.5). For the initial distribution, we used the mean density of non-smokers subjects, reflecting the "healthy" situation.
As stated in the introduction, in our model there are two types of subjects : those who are healthy and those who are affected by COPD. We make the assumption that these two situations can be represented by the same model, but with different parameter values. To be able to simulate the model, it is necessary to obtain numerical values for these parameters. This will be achieved through biological experiments and data from literature. We denote by γ^{ctl} (resp. γ^{COPD}) the value of the parameter γ for a healthy (resp COPD) subject.
All the parameters are defined below and summarized in Table 1 in Section 6.

2.1.2 Representation of the surface of interest

We consider a lattice, of dimension 103×103 where the area of each square is determined by the size of a cell (Figure 1). A C cell has a diameter of about 8 μm ([35] and our unpublished observations), giving a surface area of 50 μm^2. The size is roughly equivalent for a F cell. Thus, the cells are modeled by squares with a side length $x_0 = 7$ μm, which correspond to the units of the lattice. Each element of the lattice is defined by 2 coordinates, where the point on the upper left (resp. lower right) corner has the coordinates $(1, 1)$ (resp. $(103, 103)$). The coordinates of the center of the lattice are $(52, 52)$. The geometry of bronchi corresponds to the transverse section of a cylinder, then we model our surface of interest, the peribronchial (also called « lamina propria »), by a crown with a "hole" in the middle. The external and internal radii of this crown are defined thanks to our measurements on the bronchial tissues :

1. the internal radius is 263 μm, which represents the length of 38 lattice sites. This has been calculated using our measurements of the corresponding disk (i.e. lumen area + epithelium surface), which is on average 216 567 μm^2.
2. The external radius is 355 μm, which represents the length of 50 lattice sites. This has been calculated using our measurements of the corresponding disk (i.e. lumen area + epithelium surface + lamina propria), which is on average 396 436 μm^2.

Then the lamina propria $\mathcal{L}$ is the set of points with coordinates (i, j) such that :

$$38 \leq \widehat{d}\big((i, j),\ (52, 52)\big) \leq 50$$

where $\widehat{d}$ is the pseudo-distance : $\widehat{d}\big((i,j),\ (i',j')\big) = \big\lfloor \sqrt{(i-i')^2+(j-j')^2} \big\rfloor$ and $\lfloor x \rfloor$ stands for the integer part of the real number x. We thus obtain a working surface containing 3 652 lattice sites (potential cells) corresponding to an area of approximately 179 000 μm^2, which is in agreement with our *in situ* measurements. In other words, the number $|\mathcal{L}|$ of elements of $\mathcal{L}$ equals 3 652. Reflecting (zero-flux) boundary conditions are imposed at the external and internal borders. On each site, there is at most one cell.
In the literature, it is described that bronchial wall thickness is increased in COPD patients, ([20], [15]) but we did not observe this increase in our tissue measurements. We will consider the area of the lamina propria to be the same for healthy subjects and patients with COPD.

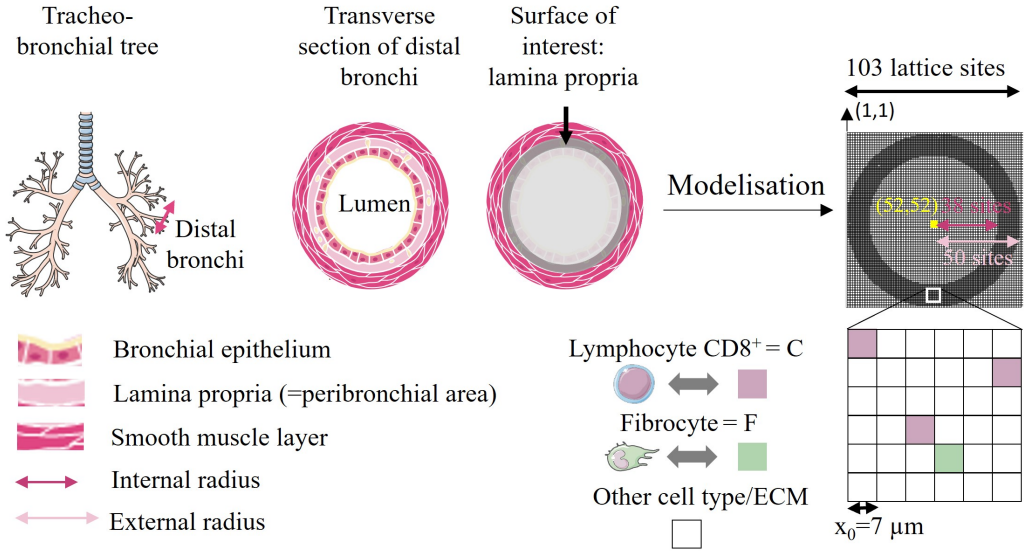

Figure 1. The lamina propria $\mathcal{L}$ forms two 2-dimensional crown shape in the bronchial wall, between the bronchial epithelium and the smooth muscle layer. ECM : extracellular matrix.

We now fix some notations.

Notation 2.1 *1. For any site $(i,j) \in \mathcal{L}$, $M(i,j)$ is the neighbourhood of (i,j), it is the set of $(i-1,j-1),(i-1,j),(i-1,j+1),(i,j-1),(i,j+1),(i+1,j-1),(i+1,j),(i+1,j+1)$ belonging to $\mathcal{L}$. For a site inside the lamina propria the cardinal of $M(i,j)$ is 8 and lower if this site is at the edge of $\mathcal{L}$. We will note in the following $|M(i,j)|$ the number of elements of $M(i,j)$. In the literature, Moore's neighbourhood is $M(i,j) \cup \{(i,j)\}$.*

2. A site of $\mathcal{L}$ has the code 1 (resp. 2) if it contains a F (resp. C) cell. If the site is empty it will be coded 0. This state corresponds either to another cell type (mainly mesenchymal, that was hypothetized to interact minimally with fibrocyte and CD8+ T cells) or to extracellular matrix, which does not play any role in the cellular cross-talk. This is the predominant state, as the bronchial wall contains structural and immune cells sparsely embedded in the extracellular matrix.

3. A configuration is an element $x = \big(x(i,j)\big)_{(i,j)\in\mathcal{L}}$ where $x(i,j)$ belongs to $\{0,1,2\}$ and $x(i,j) = 1$ (resp. $x(i,j) = 2$) means that a F (resp. C) cell occupies the site (i,j) and $x(i,j) = 0$ when the site (i,j) is empty. The set of configurations is $\{0,1,2\}^{\mathcal{L}}$ and is identified with $\{0,1,2\}^{|\mathcal{L}|}$.

4. For any $s = (i,j)$, $V(F)(s)$ (resp. $V(C)(s)$) denotes the number of F (resp. C) cells

near s

$$V(F)(s) = \sum_{s' \in M(s)} 1_{\{x(s')=1\}}, \quad V(C)(s) = \sum_{s' \in M(s)} 1_{\{x(s')=2\}}.$$

$V(s)$ *is the number of* F *and* C *cells close to* s *:*

$$V(s) = V(F)(s) + V(C)(s) = \sum_{s' \in M(s)} 1_{\{x(s')=1 \text{ or } 2\}} = \sum_{s' \in M(s)} 1_{\{x(s') \neq 0\}}.$$

2.1.3 The initial cell distribution

For the initial distribution ν_0, we first used the mean of the densities of C and F cells measured on tissues from non-smokers subjects, reflecting the "healthy" situation :

$$n_0(C) = 0.660 \times 10^{-3} \text{cells } /\mu m^2 \text{ and } n_0(F) = 0.106 \times 10^{-3} \text{ cells}/\mu m^2.$$

To obtain these densities with a lattice of 3 652 sites which represents an area of $3\,652 \times 49 = 178\,948 \approx 179\,000 \mu m^2$, we will therefore consider

$$\begin{array}{rcl} N_0(C) & = & 0.660 \times 10^{-3} \times 179\,000 \approx 118 \ C \text{ cells} \\ N_0(F) & = & 0.106 \times 10^{-3} \times 179\,000 \approx 19 \ F \text{ cells.} \end{array} \tag{2.1}$$

Second we choose the $N_0(C)$ (resp. $N_0(F)$) C (resp. F) cells uniformly distributed in the lamina propria.
Random spatial representations can be obtained with determinantal point processes. We have not retained them because they rather model repulsive phenomenons and therefore they are not adapted to our interaction model. Moreover their simulation is delicate, see [26].

2.1.4 Cell death

C and F cells have a limited lifespan, which varies from cell to cell. When they are alive, they will be able to move or duplicate as explained in the following sections. In our algorithm (see Section 2.1.10), when a cell dies, it stays in place for a while and then disappears.
We suppose that a F cell has a probability p_{dF} of dying, see Figure S1.
We define for each C cell a "basal" probability p_{dC} of dying, and an increased probability p_{dC+} of dying when the C cell has many other C cells in its neighbourhood. We distinguish two cases see Figure S1 :

1. if C cell has few C neighbours ($V(C)(s) < \sigma$, where σ is an unknown integer), then this C cell attemps to die with the probability p_{dC}
2. If C cell has many C neighbours ($V(C)(s) \geq \sigma$), then C cell attemps to die with the probability p_{dC+}.

The introduction of the probability p_{dC+} is justified by a recent study ([55]) showing the existence of CD8+ T cell-population-intrinsic mechanisms regulating cellular behavior, with induction of apoptosis to avoid an excessive increase in T cell population. Therefore, we defined σ, as the threshold number of neighbouring C cells, above which the probability of dying for a C cell is increased from p_{dC} to p_{dC+}.
The numerical values of p_{dC}, p_{dC+}, σ and p_{dF} will be presented in Section 3.1.1.

2.1.5 Proliferation of C cells

Cells have the ability to duplicate. In our algorithm (see Section 2.1.10), when a cell divides, it gives birth to 2 daughter cells, with one staying at the place of the mother cell, and the other one being created in an empty site in the neighborhood of the mother cell. We define for each F cell a probability p_F of dividing. Based on our own unpublished observations and published studies ([29] and [46]), fibrocytes (F cells) very poorly proliferate in culture, allowing us to consider that an F cell does not divide in lung tissue. We will thus consider that a F cell does not proliferate, so we will take $p_F = 0$.
For each C cell, we define a "basal" probability p_C of dividing and an increased probability $p_{C/F}$ of dividing when the C cell has F cell(s) in its neighbourhood. This latter probability is justified as our unpublished results and those from another study ([1] et al., 2021) show a robust and high increase of C cell proliferation in direct co-cultures of F and C cells.
Consider a C cell located in s (Figure S2). To reflect contact inhibition that enables cells to stop proliferating when many of them are in contact with each other, we also introduce the threshold number λ, such that the proliferation of C does not occur if for any s' neighbouring s, the number of C cells exceeds λ.

1. In the following two cases
   (a) all sites in $M(s)$ are occupied (i.e. $V(s) = |M(s)|$)
   (b) if all empty s' sites belonging to $M(s)$ have "many" C neighbours (i.e. $V(C)(s') \geq \lambda$, where λ is an integer to be specified)

   the C cell does not divide.
2. There exists at least one empty site $s' \in M(s)$ such that $V(C)(s') < \lambda$.
   (a) If there is no F cell in $M(s)$, the C cell attempts to divide with the probability p_C.
   (b) If there is at least one F cell in $M(s)$, the C cell attempts to divide with the probability $p_{C/F}$.

   If proliferation occurs, we decide that C remains in s and we uniformly choose an unoccupied site s' belonging to $M(s)$, such that $V(C)(s') < \lambda$, on which we create a new cell.

Since in the absence of stimulation, the major part of C cells do not divide in the lung ([18]), we will therefore consider that in the absence of any other stimulation, the probability p_C that a C cell divide in the peribronchial area is zero, for control subjects as well as COPD patients :

$$p_C^{ctl} = p_C^{COPD} = 0. \tag{2.2}$$

Previous studies indicate that the doubling time of C cells *in vivo* after a stimulation such as a contact with a fibrocyte is estimated around $4h$ ([54], [27]). We will consider an average duration of $4h = 80 \times 3min$ for a cell cycle of a C cell when a F cell is in its close environment. For healthy subjects, the increased probability $p_{C/F}$ of dividing will therefore be taken equal to 1/80. This probability is identical for control subjects and COPD patients :

$$p_{C/F}^{ctl} = p_{C/F}^{COPD} = 1/80 = 1.25 \times 10^{-2}. \tag{2.3}$$

2.1.6 Displacement of C and F cells

C and F cells are able to move, as shown previously ([6], [35]). This process is taken into account in the model, as described below.
Let $s = (i, j)$ and $s' = (i', j')$ be two sites of the lamina propria. A cell can only move to a site adjacent to the occupied site :

$$P_F(s, s') = P_C(s, s') = 0 \text{ if } s' \notin M(s) \cup \{s\} \text{ or } s' \in M(s) \text{ and is occupied}$$

where $P_F(s, s')$ (resp. $P_C(s, s')$) denotes the probability that a F (resp. C) cell has to move from s to s'.
Our chemotaxis experiments show that F cells are significantly attracted towards the secretion of C cells, whatever the condition of the subject (control or COPD). This leads us to take

$$P_F(s, s') = \begin{cases} k_F f_F\big(V(C)(s')\big) & \text{if } s' \in M(s) \text{ and } s' \text{ is empty} \\ k_F x_F & \text{if } s' = s \end{cases} \tag{2.4}$$

where $x_F > 0$, f_F is a function defined on $\{0, 1, 2, \cdots, 8\}$ taking positive values and

$$k_F = \frac{1}{x_F + \sum_{s' \in M(s)} f_F\big(V(C)(s')\big) 1_{\{s' empty\}}} \tag{2.5}$$

is the normalization factor such that $P_F(s, \cdot)$ is a probability.
Since this chemotactic effect requires soluble factors that have to be secreted in a sufficient concentration, this justifies an almost zero attraction ($\epsilon_F > 0$ "small", arbitrarily chosen as $\epsilon_F = 10^{-3}$) for s' such as $V(C)(s') < 3$ cells and a maximal and constant attraction for s' such as $V(C)(s') = 3$ or 4 cells. On the other hand, the attraction of the site s' for a F cell probably decreases when the site is too "crowded", because of physical hindrance and/or the secretion of factors that are secreted when many C cells are aggregated. For control subjects, we have thus chosen $f_F^{ctl}(n) = 1$ (resp. $f_F^{ctl}(n) = \epsilon_F$) if $n \in \{3, 4\}$ (resp. $n \in \{0, 1, 2, 5, 6, 7, 8\}$).
Our chemotaxis experiments show that secretions from C cells isolated from parenchyma of COPD patients are more attractive for F cells than those of C cells isolated from control patients, indicating that a smaller number of C cells is required to attract F cells in pathological condition than in healthy situation. For patients with COPD, we have thus chosen : $f_F^{COPD}(n) = 1$ (resp. $f_F^{COPD}(n) = \epsilon_F$) if $n \in \{2, 3, 4\}$ (resp. $n \in \{0, 1, 5, 6, 7, 8\}$).
We now consider the case of a C cell alive and occupying the site s. It will move to the site $s' \in M(s) \cup \{s\}$, with probability

$$P_C(s, s') = \begin{cases} k_C f_C\big(V(s')\big) & \text{if } s' \in M(s), s' \text{ is empty} \\ k_C x_C & \text{if } s' = s \end{cases} \tag{2.6}$$

with $x_C > 0$, f_C is a function defined on $\{0, 1, 2, \cdots, 8\}$ taking positive values and

$$k_C = \frac{1}{x_C + \sum_{s' \in M(s)} f_C\big(V(s')\big) 1_{\{s' empty\}}} \tag{2.7}$$

is the normalization factor such that $P_C(s, \cdot)$ is a probability.
Based on the same type of justifications than those used for F cells, f_C^{ctl} is the function defined on $\{0, 1, 2, 5, 6, 7, 8\}$ such that $f_C^{ctl}(n) = 1$ (resp. $f_C^{ctl}(n) = \epsilon_C$ where $\epsilon_C = 10^{-3}$) if $n \in \{4, 5\}$ (resp. $n \in \{0, 1, 2, 3, 6, 7, 8\}$). We will consider that f_C is identical in control subjects and COPD patients, leading to $f_C^{ctl} = f_C^{COPD}$, see Figure S4.
The values of x_F and x_C will be determined in Section 3.1.2.

2.1.7 Infiltration of C and F cells at the stable state

F and C cells can infiltrate the lungs at the stable state, as justified below.
F cells have a limited lifespan in the lungs, with a half-life that we have estimated at 10 months in the lung, by analogy with the half-life of interstitial macrophages ([47]). Our previous work (cf [7]) indicates presence of F cells in the lungs, at varying densities in control subjects and COPD patients, suggesting infiltration of F cells at stable state, in order to maintain this pulmonary pool relatively constant. This leads us to add F cells, for an healthy subject as for a COPD subject, to reflect infiltration into the lungs at the stable state.
Since C cells have a limited lifespan in the airways, with an estimated half-life of 14 days in the lung ([34]), it has been proposed that the number of memory C cells in the lung tissue is maintained through continuous recruitment ([8] and [51]).
We will add at the beginning of each $3mn$ time step, one F (resp. C) cell with probability p_{istaF} (resp. p_{istaC}) to take into account the phenomenon of infiltration during the stable state. These probabilities will be determined from biological considerations (see Section 3.1.3). The choice of the value of $3mn$ will be justified later in Section 2.1.9. If a cell is recruited, we randomly and uniformly position it among the empty sites. If there are no empty sites, no cell is added.

2.1.8 Infiltration of F and C cells during exacerbations

The process of infiltration can be amplified during exacerbations, which is an acute event specific of patients with COPD, and which is not happening in healthy subjects.
Concerning F cells, in COPD patients, there is an increase in the concentration of F cells in the blood during exacerbations ([6]). In the lungs, the density of F cells is higher in tissues of COPD patients than in those of healthy subjects ([7]), suggesting that for COPD patients, F cells are recruited from the blood to the lungs at the time of exacerbations. The average frequency of exacerbations is one per year in patients with COPD ([21]). To take into account the excess of F cells infiltration during this particular event, we will add, each year, a number $N(iexaF)$ of F cells, with the probability p_{iexaF} so that after 20 years, on average, the number of F cells in COPD patients is double than in healthy patients. If cells are added, they are placed uniformly on the empty sites of the lamina propria.

Concerning C cells, the literature shows that there is probably an infiltration of C cells in the lungs, especially in COPD patients ([9] and [43]), but whether this infiltration occurs during exacerbations is not entirely clear. A study evidences an increased level of CD8+ T cells in the blood during exacerbations, which is interpreted as extravasation of CD8+ T cells towards sites of inflammation and lymphoid organs ([9]), while another publication highlights an increased number of CD8+ T cells in the blood of COPD patients during exacerbation ([4]). In a mice model of viral exacerbation, an increase of up to 5 times in the number of lung CD8+ T cells was observed 4 days after infection, before quickly returning to normal 6 days after infection ([8]).Overall, there therefore seems to be an infiltration of CD8+ T cells during exacerbations, however this infiltration seems to be very transient. For simplification, we will assume that there is no C cell infiltration during exacerbations. Thus, for a healthy subject as well as for a patient with COPD the value of p_{iexaC} is zero.

2.1.9 The different time scales

Let v_0 be the median speed of a C cell measured in lung tissue during 15 minutes, and its value has been fixed accordingly to experimental measurements ([35]). In this study, CD8+ T cells have been imaged and tracked in mice lungs using two-photon live imaging. During the 15 min time frame which is typically used to analyze T cell movement, CD8+ T cells have been found to move at a median speed of 2.3 $\mu m/mn$. This value is also consistent with other experimental measurements ([17]). Therefore, we choose :

$$v_0 = 2.3\ \mu m/mn. \tag{2.8}$$

Since we have no information on the *in vivo* speed of a F cell, we will assume that its speed is identical to that of a C cell. For an idealized cell modeled by a square with a side length $x_0 = 7\ \mu m$, v_0 thus represents approximately a movement of one square (lattice site) every $t_0 = 3$ minutes. We therefore set the duration of a time step to 3 min.
The time steps are denoted k, where $1 \leq k \leq T$ and T is the time it takes between the beginning of cigarette smoke exposure and the onset of the disease. The development of COPD takes several decades ([31]), we therefore choose arbitrary T equal to 20 years. As the time step in our model is $3min$, T is expressed in iterations, and the value of T is :

$$T = 20 \times 365 \times 24 \times 20 = 3\ 504\ 000\ iterations$$

To take into account cell death, proliferation, displacement, duplication of cells we use the procedure given in Section 2.1.10 : we divide each time step k in N_k sub-time steps, where N_k is the number of cells at the beginning of time step k. At each sub-time step, a cell is drawn at random and can die, proliferate or move. We will consider more finely that v_0 is a median in Proposition 3.2.

2.1.10 The dynamics of C and F cells

Let us consider the beginning of the time step $k+1$. There are $N_k(F)$ F cells and $N_k(C)$ C cells, then $N_k = N_k(C) + N_k(F)$. If a C or F cell is added by infiltration at the stable state (cf subsection 2.1.7) we consider however that it is not part of the N_k initial cells, and cannot be drawn at random afterwards. It is therefore neither subject to death, nor to proliferation, nor to displacement during the time step $k+1$, it is just considered as present.
We divide the time step $k+1$ into N_k sub-time steps. For each sub-time step, we randomly draw a cell among the N_k present (with the probability $1/N_k$). Several cases can occur.

1. If the selected cell is dead or if it is a C cell that gave birth to a new cell by proliferation in a previous sub-time step, nothing happens.
2. Assuming in the following that the selected cell is alive and is not a "mother" cell, we denote by (i, j) the site occupied by this cell. The cell attempts to die following the procedure described in Subsection 2.1.4.
3. Suppose that the randomly drawn cell does not die.
   (a) If the selected cell is F, it moves according to the rule described in Section 2.1.6.
   (b) If it is a C cell,
      i. it divides according to the procedure described in Section 2.1.5. If the cell proliferates, we consider that the cell that has been added is not part of the population of N_k cells ;

ii. otherwise, it moves according to the rule described in Section 2.1.6.

When the N_k subtime steps have been repeated independently we add to the initial population cells that are either born by proliferation or recruited by infiltration. Dead cells are removed. The number of cells is then N_{k+1}. We start a new cycle of N_{k+1} sub-time steps, as previously described. Therefore, over a time step, a given cell will on average die, move or divide (if it is a C cell).

Infiltration during exacerbation : Every year, i.e. after 175 200 time steps, we add a number $N(iexaF)$ of F cells with the probability p_{iexaF}. If F cells are recruited by infiltration during an exacerbation, they are randomly and uniformly positioned among all of the vacant sites. Cells that have infiltrated in the meantime are added to the initial population. A new time step starts again as described above.

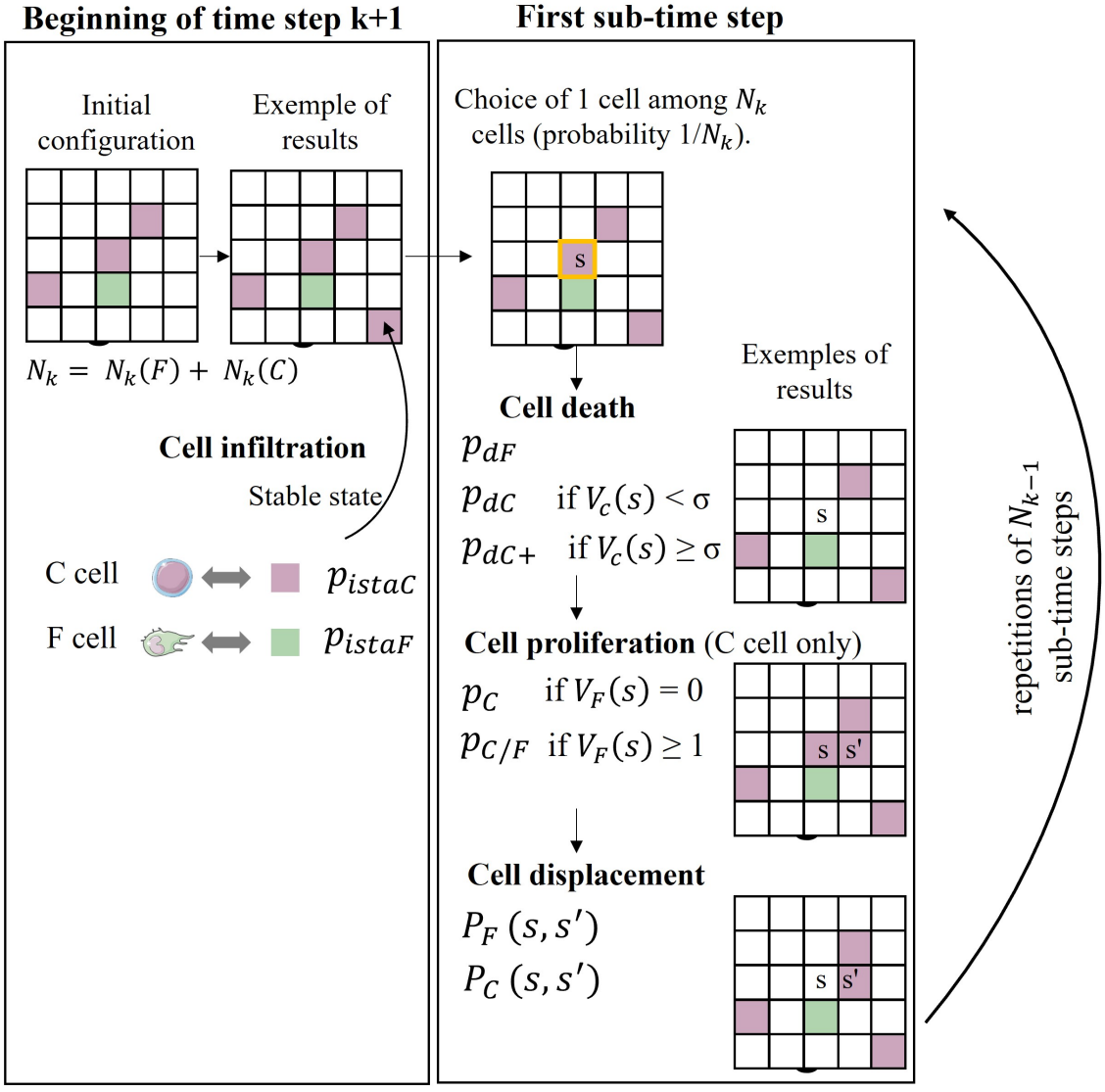

Figure 2. Algorithm defining cell infiltration, death, proliferation and displacement of cells at each time step. We consider the beginning of the time step $k+1$. This period is divided into N_k sub-time steps, where N_k is the number of cells at the beginning of period $k+1$. F and C

cells are indicated by respectively green and purple squares.

2.2 Markov property

We start by setting some notations.

Definition 2.2 *1. For any k belonging to $\{1, \cdots, T\}$, $X_k = \big(X_k(i,j)\big)_{(i,j)\in\mathcal{L}}$ represents the state of the lamina propria at the end of the k time step. According to item 3 of Notation 2.1, $X_k(i,j) = 1$ (resp. $X_k(i,j) = 2$) means that a F (resp. C) cell occupies the site (i,j) and $X_k(i,j) = 0$ when the site (i,j) is empty. X_k is a random variable which takes its values in $\{0,1,2\}^{\mathcal{L}}$.*

2. ν_0 is the distribution of the initial state X_0, its value will be given in Section 2.1.3

3. Let $N_k(C)$ (resp. $N_k(F)$) be the number of C (resp. F) cells at the end of time step k.

We adopt the notations used in the theory of random processes : for any initial probability μ on $\{0,1,2\}^{\mathcal{L}}$, $\mathbb{P}_\mu$ represents the probability under which the law of X_0 is μ.

Proposition 2.3 *$(X_k)_{k\geq 0}$ is a recurrent, irreducible, a-periodic Markov chain that admits an unique invariant probability ν.*

Proof. Note that

$$N_k(F) = \sum_{(i,j)\in\mathcal{L}} 1_{\{X_k(i,j)=1\}}, \quad N_k(C) = \sum_{(i,j)\in\mathcal{L}} 1_{\{X_k(i,j)=2\}}.$$

Therefore, if $x = X_k$ is known, the quantities $N_k(F)$ and $N_k(C)$ are fixed, as well as the composition of each neighbourhood. It is then possible to write $X_{k+1} = F(X_k, \xi)$, where F is a function and $\xi = (\xi_i)_{i\geq 1}$ is a sequence of independent random variables and with uniform law on $[0,1]$, independent of X_k. The Markovian property is immediately deduced from this. It is straighforward to prove that the Markov chain is recurrent and irreducible. Since $\mathbb{P}_x(X_1 = x) > 0$, for any x, it is a-periodic. Therefore $(X_k)_{k\geq 0}$ admits a unique invariant probability. ■

To obtain the equilibrium state during simulations, one could think of using the Prott algorithm which allows to carry out exact simulations, see the seminal paper [41]. The lamina propria has a finite number of sites but too many (3 652), this algorithm only works when a "sandwiching" hypothesis is realized, see Chap. 11 in [13]. Unfortunately, in our context this assumption is not satisfied.

Corollary 2.4 *Let μ be an initial law on $\{0,1,2\}^{\mathcal{L}}$. The two sequences of random variables $\big(N_k(F)\big)_{k\geq 0}$ and $\big(N_k(F)\big)_{k\geq 0}$ converge in law when k tends to infinity. Moreover there is convergence of the means :*

$$\lim_{k\to\infty} \mathbb{E}_\mu\big(N_k(F)\big) = \mathbb{E}_\nu\big(N_0(F)\big), \quad \lim_{k\to\infty} \mathbb{E}_\mu\big(N_k(C)\big) = \mathbb{E}_\nu\big(N_0(C)\big).$$

Proof. We only deal with F cells. Note that $\mathbb{P}_\mu\big(N_k(F) = l\big) = \mathbb{P}_\mu\big(X_k \in A(l,F)\big)$, where l is an integer and $A(l,F) = \Big\{x,\ \sharp\big\{(i,j) \in \mathcal{L}, \text{ such that } x(i,j) = 1\big\} = l\Big\}$. We deduce the

convergence in law of $N_k(F)$, as $k \to +\infty$. Moreover :

$$\begin{aligned}\lim_{k\to\infty} \mathbb{E}_\mu\big(N_k(F)\big) &= \lim_{k\to\infty} \Big(\sum_{l=0}^{|\mathcal{L}|} l\ \mathbb{P}_\mu\big(X_k \in A(l,F)\big)\Big) \\ &= \sum_{l=0}^{|\mathcal{L}|} l\ \mathbb{P}_\nu\big(X_k \in A(l,F)\big) = \mathbb{E}_\nu\big(N_k(F)\big) = \mathbb{E}_\nu\big(N_0(F)\big).\end{aligned}$$

■

Since we are interested in a large number of periods $T \approx 3.5 \times 10^6$ time-steps, we can consider that the Markov chain has reached its stationary state. This state depends only on the parameters and is independent from the initial distribution of cells.

2.3 The streamlined model

The streamlined model is a special case of the model, where local interactions, *i.e.* C cell-induced cell death and contact inhibition of C cell proliferation play no role. To reflect these two properties, σ and λ have been fixed respectively to 9 and 0. In the streamlined model, the probability p_C that a C cell divide is zero (see justification below). In the streamlined model the parameters are :

$$\sigma = 9, \quad p_C = 0, \quad \lambda = 0. \tag{2.9}$$

This means that C and F cell displacement, the stable infiltration and that due to exacerbations (see Section 2.1.7, resp. 2.1.8) are identical to those in the complete model. However, C cells do not proliferate at all (i.e. $p_C = 0$ and $\lambda = 0$) and die with the probability p_{dC} independently of the local context ($\sigma = 9$).
Since the streamlined model is a special case of the interaction model, the results of Section 2.2 apply. In particular, the streamlined model is Markovian.
The major interest of the streamlined model is that it allows a rigourous mathematical analysis to accurately calculate parameters such as v_0, p_{dC}, p_{dF}, x_C, x_F, p_{istaC}, p_{istaF}, p_{iexaF} and N_{iexaF}.
We now justify the choice $p_C = 0$. Indeed, the cell cycle length of a C cell is highly variable, and it is difficult to obtain quantitative data at steady state. In so-called "nonlymphoid" tissues, such as the peribronchial area, activated C cells are unable to divide, although they are able to do so in vitro in response to the same antigenic stimulus ([14]). After primary viral infection, a minor part of the memory C cells continues to proliferate in the secondary lymphoid organs after resolution of the infection, and are recruited in the lungs, which makes it possible to ensure a relatively constant quantity of memory C cells in the lungs ([18]). The major part of the antigen-specific memory effector C cells no longer divides in the lung. We will therefore consider that in the absence of any other stimulation, the probability p_C that a C cell divide in the lamina propria is zero.

2.4 Algorithm implementation

Our algorithm (see section 2.1.10) is implemented in Julia, which allows to parallelize the computation sequences as well as to use graphic libraries, in order to produce drawings and

videos illustrating step by step the evolution of a starting situation according to the biological parameters selected to launch the simulations. Our program is modular, in the sense that it is made up of reusable functions for the benefit of users wishing to test other configurations involving different evolutionary laws. A complete version of the program can be downloaded from the following site :

`https://plmbox.math.cnrs.fr/d/49bcbc1db63a4654be7e`

3 Results

3.1 Determination of parameters via biological information

We will use the streamlined model for which a probabilistic analysis is possible to determine numerical values for the parameters ν_0, p_{dC}, p_{dF}, x_C, x_F, p_{istaC}, p_{istaF} p_{iexaF} and $N(iexaF)$ for healthy subjects and patients with COPD. We will proceed in two steps. For each parameter considered, we will start by stating a mathematical property formulated in the framework of the streamlined model. Then, the use of biological data will allow to deduce a numerical value of the parameter which will be used for the simulations. For ease of reading, the proofs are pushed back to Section 5.
The numerical values of the different parameters in the streamlined model are presented in Table 2, see Section 6.

3.1.1 Determination of p_{dC}, p_{dC+} and p_{dF}

We take into account that, for a healthy subject, the half-lives $hl(C)$ and $hl(F)$ of C and F cells are known. Half-live is defined as the time required for the death of half a cell population. Thank to cell tracing experiments in animal models, this time is relatively easy to measure. Expressing the half-life of a cell as a function of its probability of dying over a 3mn-period is however non trivial, and is rigorously described below.

We consider a F cell at time 0 or a C cell at time 0 or just born. Let us note $T(C)$ (resp. $T(F)$) the life time of a C (resp. F) cell and $q_{1/2}\big(T(C)\big)$ (resp. $q_{1/2}\big(T(F)\big)$) its median. Recall that the median of a probability law is its quantile of order $1/2$.

Proposition 3.1 *We have*

$$\Big\lfloor \frac{\ln 2}{\ln\big\{1/(1-p_{dC})\big\}} \Big\rfloor \;\leq\; q_{1/2}\big(T(C)\big) \leq 1 + \frac{\ln 2}{2(1-p_{dC})^2} + \Big\lfloor \frac{\ln 2}{\ln\big\{1/(1-p_{dC})\big\}} \Big\rfloor \tag{3.1}$$

$$\Big\lfloor \frac{\ln 2}{\ln\big\{1/(1-p_{dF})\big\}} \Big\rfloor \;\leq\; q_{1/2}\big(T(F)\big) \leq 1 + \frac{\ln 2}{2(1-p_{dF})^2} + \Big\lfloor \frac{\ln 2}{\ln\big\{1/(1-p_{dF})\big\}} \Big\rfloor \tag{3.2}$$

where $\lfloor x \rfloor$ is the greatest integer less than or equal to x.

Equation (3.1) (resp. (3.2)) gives a lower and an upper bound of the quantile of the half-life of a C (resp. F) cell. It effectively allows to determine a value of p_{dC} (resp. p_{dC}) as explained below. Indeed, it is known from the literature ([34] and [47]) that

$$hl^{ctl}(C) = 14 \text{ days } = 6\,720 \text{ time steps}, \quad hl^{ctl}(F) = 10 \text{ months } = 144\,000 \text{ time steps}. \tag{3.3}$$

We choose p_{dC} such that $hl^{ctl}(C) = \frac{\ln 2}{\ln\left\{1/(1-p_{dC})\right\}}$ and p_{dF} so that $hl^{ctl}(F) = \frac{\ln 2}{\ln\left\{1/(1-p_{dF})\right\}}$, *i.e.*

$$p_{dC}^{ctl} = 1 - e^{-\ln 2/hl^{ctl}(C)} \approx 1.0 \times 10^{-4}, \quad p_{dF}^{ctl} = 1 - e^{-\ln 2/hl^{ctl}(F)} \approx 4.8 \times 10^{-6}. \tag{3.4}$$

For this choice of p_{dC}^{ctl} and p_{dF}^{ctl} we have : $\dfrac{\ln 2}{2(1-p_{dC}^{ctl})^2} \approx 0.151$ and $\dfrac{\ln 2}{2(1-p_{dF}^{ctl})^2} \approx 0.151$.
We can thus deduce that the median of $T(C)$ (resp. $T(F)$) is reasonably close to $hl^{ctl}(C)$ (resp. $hl^{ctl}(F)$).
A study [49] suggests a modification of the C cell death processes in tissues from patients with COPD, with a decrease by about half of the percentage of apoptotic C cells in the distal airways of mild to moderate COPD patients, which constitute the majority of our study cohort. In patients with COPD, we will therefore choose for each C cell the probability p_{dC}^{COPD} of dying equal to

$$p_{dC}^{COPD} = p_{dC}^{ctl}/2 \approx 5 \times 10^{-5}. \tag{3.5}$$

Our previous work [7] showed that the exposure of fibrocytes to the secretions of the bronchial epithelia from patients with COPD decreases by a factor 2 the percentage of dead cells . Therefore we choose :

$$p_{dF}^{COPD} = p_{dF}^{ctl}/2 \approx 2.4 \times 10^{-6}. \tag{3.6}$$

In the streamlined model, which is a special case where local interactions play no role, σ is equal to 9 neighbors.
Studies show that lymphocyte cell death is increased by a factor 4 in a crowed environment ([45], [55]). We therefore choose : $p_{dC+} = 4p_{dC}$. We thus obtain :

$$p_{dC+}^{ctl} = 4p_{dC}^{ctl} \approx 4.0 \times 10^{-4}, \quad p_{dC+}^{COPD} = 4p_{dC}^{COPD} \approx 2.0 \times 10^{-4}. \tag{3.7}$$

3.1.2 Determination of x_C and x_F

The parameters x_F and x_C are terms involved in the definition of respectively $P_F(s, s')$ and $P_C(s, s')$, see (2.4) and (2.6). They are chosen such as the median speed of F and C cells is equal to 2.3 $\mu m/mn$, as describe below.
Since C and F cells behave in a similar way, we will detail the following analysis only for F cells. Let $\alpha > 0$ be a real number such that

$$\mathbb{P}(Y_\alpha \leq 4) = \frac{1}{2}, \quad \text{where } Y_\alpha \sim \mathcal{P}(\alpha). \tag{3.8}$$

It is easy to determine numerically the value of α, we find $\alpha \approx 4.67091$.
Consider a F cell occupying the site s and which is alive and not completely surrounded. According to (2.4), F moves with probability $p_{moveF} = 1 - k_F x_F$. Since $\alpha < 5$, we can easily deduce from relation (2.5) that there is a unique x_F such that

$$p_{moveF} = 1 - k_F x_F = \frac{\alpha}{5} \approx 0.9342. \tag{3.9}$$

This leads to :

$$x_F = \frac{1-\alpha/5}{\alpha/5}\Big(\sum_{s' \in M(s)} f_F\big(V(C)(s')\big)1_{\{s' empty\}}\Big),\ k_F = \frac{\alpha/5}{\sum_{s' \in M(s)} f_F\big(V(C)(s')\big)1_{\{s' empty\}}}.$$

(3.10)

It is now possible to take into account the biological observation (2.8). During the 15 $mn = 5\times3$ mn time intervals the F cell covers the distance of $x_0 Z$ μm where $Z = Z_k(moveF) + \cdots + Z_{k+4}(moveF)$ is the number of moves between the time steps $k+1$ and $k+5$ (recall from Section 2.1.2 that $x_0 = 7$ μm). It follows from Proposition 3.2 below that the law of Z is approximatively $\mathcal{P}(\alpha)$. The speed of F is thus $V(moveF) = \frac{x_0 Z}{15}$ $\mu m/mn$. Using (2.8) and (3.8) we get :

$$\mathbb{P}_{\nu_0}\big(V(moveF) \leq v_0\big) = \mathbb{P}_{\nu_0}(Z \leq 4.93) = \mathbb{P}_{\nu_0}\Big(Z \leq 4\Big) = \frac{1}{2}.$$

Because the streamlined model is simple, we can give in Proposition 3.2 an accurate estimation of the law of Z. During a subperiod, if F is chosen, does not die and is completely surrounded, it cannot move, but we agree that it can have a virtual move with probability $\alpha/5$. We note $Z_k(moveF)$ (resp. $Z'_k(moveF)$) the number of real (resp. real and virtual) moves during the time-step $k+1$. It is interesting to introduce the random variable $Z'_k(moveF)$ since its law under $\mathbb{P}^{|k}_{\nu_0}$ is $\mathcal{B}\Big(N_k, \frac{(1-p_{dF})\alpha}{5N_k}\Big)$, where

$$\mathbb{P}^{|k}_{\nu_0} \text{ is the conditional expectation given } X_k. \tag{3.11}$$

Proposition 3.2 *We have :*

$$\mathbb{P}^{|k}_{\nu_0}\big(Z_k(moveF) \neq Z'_k(moveF)\big) \leq \frac{1}{N_k}\mathbb{E}^{|k}_{\nu_0}\big(\Gamma_k(F)\big) \tag{3.12}$$

where Γ_k is the number of times F is fully surrounded during the time step $k+1$.

We took $k = 5$ years $= 876\ 000$ time periods, because we estimated that beyond this date the stationary state is reached. We considered an additional period and we performed 100 simulations of this scheme. For each simulation, $\Gamma_k(C) = \Gamma_k(F) = 0$ and the empirical mean of the $2/N_k$ is 0.015.
From (3.12) we deduce that the conditional law of the random variable $Z_k(moveF)$ is approximatively $\mathcal{B}\Big(N_k, \frac{(1-p_{dF})\alpha}{5N_k}\Big)$. The distance between the binomial law $\mathcal{B}(a,b)$ and the Poisson distribution $\mathcal{P}(ab)$ is lower than $\delta = 2\min(2, ab)b$ (see the Prohorov's inequality, section III.7 in [48]). In our case $\delta \leq 2/N_k$. Relations (3.4), (3.5) and (3.6) as well as our 100 simulations imply that the binomial distribution $\mathcal{B}\Big(N_k, \frac{(1-p_{dF})\alpha}{5N_k}\Big)$ can be accurately approximated by the Poisson distribution $\mathcal{P}(\alpha/5)$.

Remark 3.3 *For the C cells, there is a formula similar to* (3.12) *which is obtained by replacing the letter F by C. The real numbers x_C and k_C are given by*

$$x_C = \frac{1-\alpha/5}{\alpha/5}\Big(\sum_{s' \in M(s)} f_C\big(V(s')\big)1_{\{s' empty\}}\Big),\ k_C = \frac{\alpha/5}{\sum_{s' \in M(s)} f_C\big(V(s')\big)1_{\{s' empty\}}}. \tag{3.13}$$

3.1.3 Determination of p_{istaF} and p_{istaC}

Recall that according to Corollary 2.4, for k large enough

$$\mathbb{E}_{\nu_0}\big(N_k(C)\big) \approx \mathbb{E}_{\nu}\big(N_k(C)\big) = \mathbb{E}_{\nu}\big(N_0(C)\big), \quad \mathbb{E}_{\nu_0}\big(N_k(F)\big) \approx \mathbb{E}_{\nu}\big(N_k(F)\big) = \mathbb{E}_{\nu}\big(N_0(F)\big) \quad (3.14)$$

where ν is the invariant probability.
However, the mean equilibrium values $\mathbb{E}_{\nu}\big(N_0(C)\big)$ and $\mathbb{E}_{\nu}\big(N_0(F)\big)$ are unknown. We will select p_{istaC} (resp. p_{istaF}) as a function of p_{dC} and $N_0(C)$ (resp. p_{dF} and $N_0(F)$) in such a way that the number of C (resp. F) cells is close to $N_0(C)$ (resp. $N_0(F)$) at equilibrium. This result is based on a calculation of the expectation of $N_k(C)$ (resp. $N_k(F)$) in terms of k and the model parameters.

Proposition 3.4 *We suppose that there is no infiltration during exacerbations, i.e. $N(iexaF) = p_{iexaF} = 0$. Then for any k we have :*

$$\mathbb{E}_{\nu_0}\big(N_k(C)\big) = \Big(N_0(C) - \frac{p_{istaC}}{p_{dC}}\Big)(1-p_{dC})^k + \frac{p_{istaC}}{p_{dC}} + \epsilon_k^C \quad (3.15)$$

$$\mathbb{E}_{\nu_0}\big(N_k(F)\big) = \Big(N_0(F) - \frac{p_{istaF}}{p_{dF}}\Big)(1-p_{dF})^k + \frac{p_{istaF}}{p_{dF}} + \epsilon_k^F \quad (3.16)$$

where ϵ_k^C and ϵ_k^F are positive numbers such that

$$\epsilon_k^C \le \frac{p_{dC}}{2}\Big(\frac{p_{istaC}}{p_{dC}(1-p_{dC}/2)} + N_0(C)\Big), \quad \epsilon_k^F \le \frac{p_{dF}}{2}\Big(\frac{p_{istaF}}{p_{dF}(1-p_{dF}/2)} + N_0(F)\Big). \quad (3.17)$$

Remark 3.5

1. *Since $\lim_{k\to\infty}(1-p_{dC})^k = 0$ (resp $\lim_{k\to\infty}(1-p_{dF})^k = 0$), then under the assumption that p_{dC} (resp. p_{dF}) is small, the general formula (3.15) (resp. (3.16)) implies*

$$\mathbb{E}_{\nu_0}\big(N_k(C)\big) \approx \frac{p_{istaC}}{p_{dC}}, \quad \Big(resp.\ \mathbb{E}_{\nu_0}\big(N_k(F)\big) \approx \frac{p_{istaF}}{p_{dF}}\Big) \quad \text{for } k \text{ large enough.}$$

2. *For healthy patients, we want to determine the parameters p_{istaF} and p_{istaF} in such a way that $k \mapsto N_k(C)$ and $k \mapsto N_k(F)$ fluctuate little (at least at equilibrium) and remain close to $N_0(C)$ and $N_0(F)$ respectively. This leads us to take :*

$$p_{istaC}^{ctl} = p_{dC}^{ctl}\ N_0(C) = 1.18 \times 10^{-2}, \quad p_{istaF}^{ctl} = p_{dF}^{ctl}\ N_0(F) = 9.12 \times 10^{-5}. \quad (3.18)$$

   We easily deduce that we have achieved our goal : $\mathbb{E}_{\nu_0}\big(N_k(C)\big) \approx N_0(C)$ and $\mathbb{E}_{\nu_0}\big(N_k(F)\big) \approx N_0(F)$, for k large enough.

3. *In pratice, in the COPD case, we choose to keep the relation $p_{istaC}^{COPD} = p_{dC}^{COPD}\ N_0(C)$ and as p_{dC} is different in patients with COPD than in healthy subjects (cf (3.5)), we obtain $p_{istaC}^{COPD} = p_{istaC}^{ctl}/2 = 5.9 \times 10^{-3}$.*
   The case of F cells is analogous, we choose $p_{istaF}^{COPD} = p_{dF}^{COPD}\ N_0(F)$. Relation (3.6) leads to $p_{istaF}^{COPD} = p_{istaF}^{ctl}/2 = 4.56 \times 10^{-5}$.
   Therefore the average number of C (resp. F) cells, not counting those added by exacerbation, is close to $N_0(C)$ (resp. $N_0(F)$).

3.1.4 Determination of $N(iexaF)$ and p_{iexaF} for COPD patients

For simplification, we will assume that there is no C cell infiltration during exacerbations. Then $p_{iexaC} = 0$. Thus, for healthy subjects as well as for patients with COPD $p^{ctl}_{iexaC} = p^{COPD}_{iexaC} = 0$. Concerning F cells, the value of p_{iexaF} depends closely on the condition of the subject. For a healthy subject, as there is no exacerbation, this probability is zero : $p^{ctl}_{iexaF} = 0$. For patients with COPD, we add N_{iexaF} F cells with probability p_{iexaF} every year, which is the average exacerbation frequency of patients with COPD. Recall that we have made the same assumption as for stable infiltration : if we add N_{iexaF} F cells at the beginning of a year, these cells are not active immediately and they have to wait for the next time step before being active. In agreement with *in situ* measurements ([7]) the average number of F, after T time steps (i.e. 20 years), must be twice the number of F cells for a healthy subject.
According to item 2 of Remark 3.5, for an healthy subject, the expected number of F cells is close to the initial number $N_0(F)$ of F cells. Therefore the goal is to determine p_{iexaF} and $N(iexaF)$ such that

$$\mathbb{E}_{\nu_0}\big(N_T(F)\big) = 2N_0(F). \tag{3.19}$$

Let us introduce the real numbers K_1, K_2 and R' :

$$K_1 = \big(1-(1-p_{dF})^{T_y}\big)\Big(2N_0(F) - (1-p_{dF})^T\Big(N_0(F) - \frac{p_{istaF}}{p_{dF}}\Big) - \frac{p_{istaF}}{p_{dF}}\Big) \tag{3.20}$$

$$K_2 = (1-p_{dF})^{T_y-1}\big(1-(1-p_{dF})^T\big). \tag{3.21}$$

and

$$\begin{aligned} R' = \frac{1}{1-(1-p_{dF})^{T_y}}\Bigg\{ & \frac{p_{istaF}}{2(1-p_{dF}/2)} + \frac{p_{dF}}{2}\big(p_{istaF} + N(iexaF)p_{iexaF}\big) \\ & + \frac{p_{dF}(1+p_{dF})}{2}\Bigg[N_0(F) + \Big(\frac{p_{istaF}}{p_{dF}}\big(1-(1-p_{dF})^{T_y}\big) \\ & + (1-p_{dF})^{T_y-1}N(iexaF)p_{iexaF} + \frac{p_{istaF}}{2(1-p_{dF}/2)} \\ & + \frac{p_{dF}}{2}\big(p_{istaF} + N(iexaF)p_{iexaF}\big)\Big)\frac{1}{1-(1-p_{dF})^{T_y} - p_{dF}(1+p_{dF})/2}\Bigg]\Bigg\}. \end{aligned} \tag{3.22}$$

Proposition 3.6 *We choose :*

$$N(iexaF) = \Big\lfloor \frac{K_1}{K_2} \Big\rfloor + 1 \tag{3.23}$$

and

$$p_{iexaF} = \frac{1}{N(iexaF)}\frac{K_1}{K_2} \tag{3.24}$$

where $T_y = 175\,200$ is the number of time steps in a year. Then

$$0 \le \mathbb{E}_{\nu_0}\big(N_T(F)\big) - 2N_0(F) \le R' \tag{3.25}$$

Remark 3.7 *1. $N(iexaF)$ is the smallest integer such that (3.24) holds.*

2. Suppose that $p_{istaF} = p_{dF}\, N_0(F)$, then

$$\frac{K_1}{K_2} = \frac{N_0(F)\big(1-(1-p_{dF})^{T_y}\big)}{(1-p_{dF})^{T_y-1}\big(1-(1-p_{dF})^T\big)}.$$

3. *According to item 3 of Remark 3.5,* $p_{istaF}^{COPD} = 4.56\times10^{-5}$. *Then* $p_{istaF}^{COPD} = p_{dF}^{COPD}\ N_0(F)$ *and*

$$N(iexaF) = 10, \quad p_{iexaF} \approx 0.993, \quad R' \approx 4.3 \times 10^{-4}.$$

Consequently, the expected number of F *cells for COPD patients is reasonably close to* $2N_0(F)$.

3.2 Elements of simulation

Figure 3 shows the simulation results of fibrocytes and $CD8+$ T cells behaviors within the peribronchial area during 20 years, for healthy subjects and patients with COPD, obtained with the streamlined model. Initial cell densities were scaled with respect to reference values, corresponding to the mean densities experimentally measured in non-smoking subjects. All results in Figure 3 have been obtained from the simulations. Figure 3A represents snapshots of the peribronchial area with fibrocytes, and CD8+ T cells at the beginning and at the end of the simulations. The distributions of cells are non-uniform for healthy subjects as well as for COPD patients after 20 years (Figure 3A). An increased density of F cells as well as clusters of cells seems to be present in the sick condition (Figure 3A and movie 2). These properties are also visible on the movies 1 and 2. As these movies have been obtained 5 years after the beginning of the simulations, it shows that these particular repartitions are already present few years after the application of control or COPD dynamics. These movies also show important dynamic behavior, that would be difficult to reveal in any other way : some cells seem to form clusters, which are relatively dynamic structures. New clusters are formed during the 24h-time frame of the movies and others are dissolving, whereas some clusters seem relatively stable over the time frame, especially in the COPD situation.

Simulations allowed us to analyze the dynamics of cells over time. We represent in Figure 3B the fluctuations of $k \to \overline{N(C)}_k$, where $\overline{N(C)}_k$ is the empirical mean of the number of C cells for the month k. They are close to 118 in the healthy condition, which is equal to the initial number of C cells ($N_0(C) = 118$). It corroborates the theoretical results, showing that after a sufficient amount of time, the average number of C cells is close to $N_0(C)$ (cf Remark 3.5). Similar findings are found in the COPD condition.

To characterize the importance of cell death and infiltration, we plotted the number of C cells (resp F cells) that have died (Figure 3C, 3G) or infiltrated (Figure 3D, 3H) for each month. In agreement with experimental findings ([49]) taken into account in our model, cf (3.5), the death of C cells is reduced by two in COPD compared to control situation (Figure 3C). In both situations, the infiltration of C cells compensates C cell death (Figure 3D-E). Furthermore, as expected, the number $\overline{N(F)}_k$ doubles after 20 years, from the control (mean $\overline{N(F)} = 20$) to the COPD condition (mean $\overline{N(F)} = 40$) (Figure 3F). The change in $\overline{N(F)}_k$ in the COPD condition is mainly the consequence of the infiltration of F cells during exacerbations (Figure 3G-H), as shown by the cumulative numbers of F cells that have died and infiltrated (Figure 3I). This result was anticipated by our mathematical analysis, see Section 3.1.4, but the simulations allow us to show that the fluctuations are reasonable and seem to reproduce patients heterogeneity.

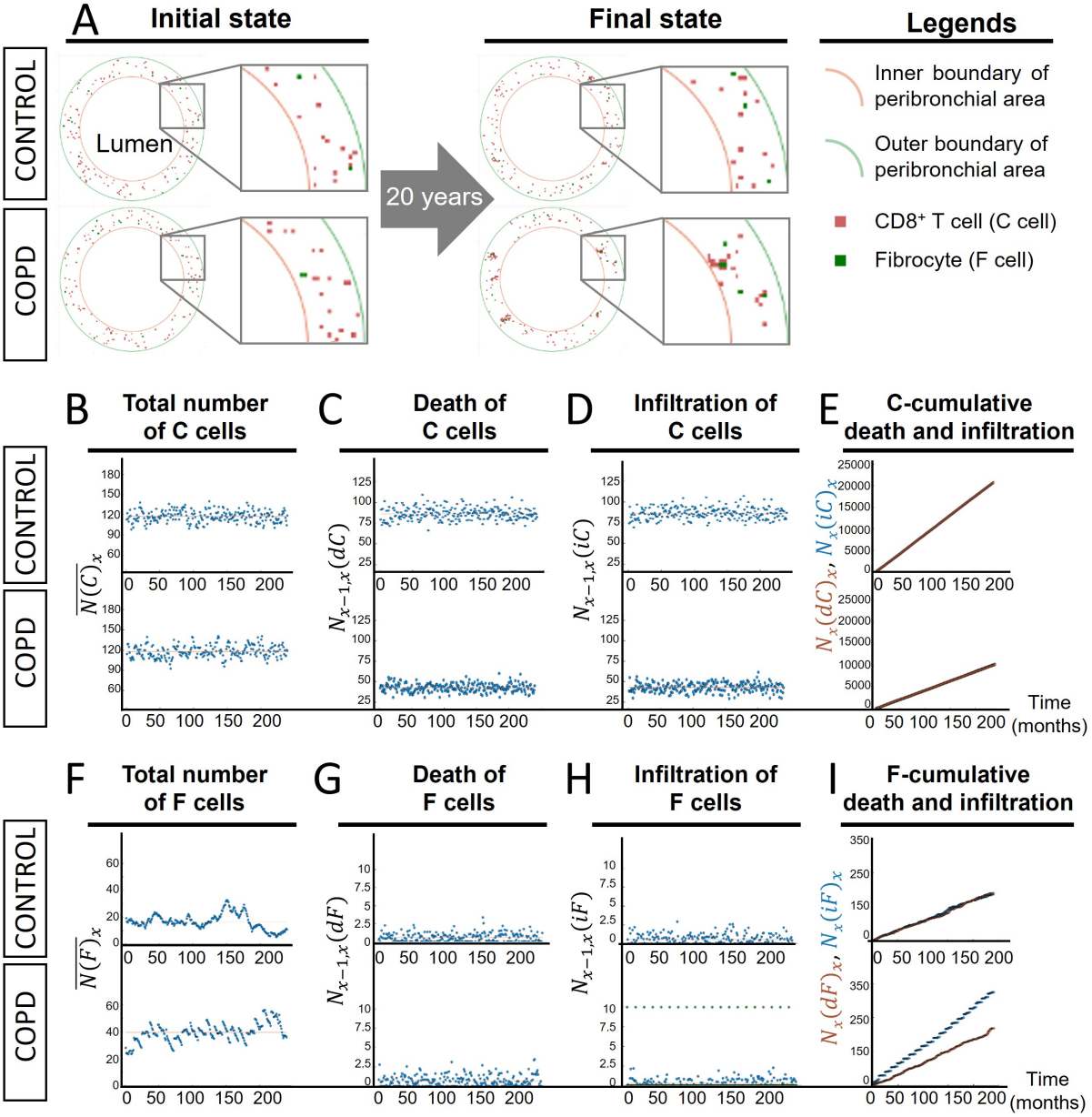

Figure 3. Simulation results of cell dynamics within the peribronchial area during 20 years, for healthy subjects and patients with COPD, obtained with the streamlined model. **A)** Selected representative pictures for control (top panels) and COPD (bottom panels) situations at initial state (left panels) and after 20 years (right panels). CD8+ T cells (C cells) and fibrocytes (F cells) are represented respectively by pink and green squares. Panels surrounded by grey : higher magnifications of peribronchial area. **B, F)** Graphs showing the time variations of $x \to \overline{N(C)}_x$ in panel B (resp. $x \to \overline{N(F)}_x$ in panel F), where $\overline{N(C)}_x$ (resp. $\overline{N(F)}_x$) is the empirical mean of the number of C (resp. F) cells for the month x. The average of $N(C)_x$ and $N(F)_x$ over the 20 years-period are indicated by red lines. **C, G)** Graphs showing the variations of $N_{x-1,x}(dC)$ (panel C) and $N_{x-1,x}(dF)$ (panel G) over time. $N_{x-1,x}(dC)$ and $N_{x-1,x}(dF)$ are the number of C (resp. F) cells that have died for the month x. **D, H)**

Graphs showing the variations of $N_{x-1,x}(iC)$ (panel D) and $N_{x-1,x}(iF)$ (panel H) over time. $N_{x-1,x}(iC)$ and $N_{x-1,x}(iF)$ are the number of C (resp. F) cells that have infiltrated the peribronchial area for the month x. The infiltration at the stable state and during exacerbation are indicated respectively in blue and green. For control situation, there is no infiltration by exacerbation. **E, I)** Cumulative distributions of the numbers of C cells $N_x(dC)$ and F cells $N_x(dF)$ that have died during the month x (red curve), and the numbers of C cells $N_x(iC)$ and F cells $N_x(iF)$ that have infiltrated the surface of interest during the month x (blue curve).

Movie legends

Cell dynamics within the peribronchial area, 5 years after the beginning the initial time, images of the simulations were recorded every 3 min during 24 hours. CD8+ T cells (C cells) and fibrocytes (F cells) are represented respectively by pink and green squares.

Movie 1 (resp. 2) : control (resp. COPD) situation.

4 Conclusion and discussion

In order to gain insights about the reasons for the breakdown of homeostasis that could emerge from slight deregulations of normal cellular processes in COPD, we developed a probabilistic cellular automaton mathematical model to replicate cell-scale properties of two different cell populations, fibrocytes and CD8+ T cells. It takes into account individual cell motility, death, proliferation and infiltration processes with rules that are dependent on the local microenvironment. We assume that the diseased and healthy states are obtained for two distinct sets of parameters. We have introduced a simpler model in which one can mathematically compute probabilities of events or expectations of random variables of interest. This allowed to accurately derive the parameters according to biologically observations in human tissues and *in vitro* experiments. The results from the simulations suggest that modifications of the parameters are sufficient to generate an increased density of fibrocytes in the COPD situation compared to the healthy one, as well as different spatial distributions, which are consistent with *in situ* observations. This has not been achieved using any experimental approaches previously.

Several assumptions were made to simplify this initial model. Parameters were estimated from biological data using the streamlined model, and their validity in the complete model is unknown. Our Markov model does not take into account memory effects, which could play a role in disease onset and evolution. In addition, cell interactions inside tissues are far more complex than those considered in this system. In particular, it does not take into account all the other cells, such as epithelial cells, smooth muscle cells and other immune cells. Long-range effects, such as the attractive effect of the bronchial epithelium at the lumen border could be included by assigning different displacement probabilities based on the distance to the inner edge of the grid. Nevertheless, our model seems to us to be a very good starting version that we may improve.

This model does not only propose causal explanations for *in situ* observations, but we also anticipate it to be predictive. Promising perspectives of this study include the ability to test the reversibility of the pathological state, as well as the efficacy and therapeutic window of a potential treatment for COPD.

5 Proofs of technical points

5.1 Proof of Proposition 3.1

Since the cells C and F play symmetrical roles, it is sufficient to consider a fixed C cell. We start with two preliminary lemmas 5.1 and 5.3.

Lemma 5.1 *Let $D_k(C)$ be the event "C dies during N_k sub-time steps of the time step $k+1$". Then*

$$P_{\nu_0}^{|k}\big(D_k(C)\big) = 1 - \Big(1 - \frac{p_{dC}}{N_k}\Big)^{N_k}. \tag{5.1}$$

and

$$p_{dC} - \frac{p_{dC}^2}{2} \leq P_{\nu_0}^{|k}\big(D_k(C)\big) \leq p_{dC}. \tag{5.2}$$

where $P_{\nu_0}^{|k}$ has been defined by (3.11).

Proof. To simplify the notations we denote by $\mathbb{P} = P_{\nu_0}^{|k}$. Let B_j be the event : "C is alive and does not die at the sub-time step j", $1 \leq j \leq N_k$. Then,

$$\mathbb{P}\big(B_j \big| B_1 \cap \cdots \cap B_{j-1}\big) = \frac{N_k - 1}{N_k} + \frac{1}{N_k}(1 - p_{dC}) = 1 - \frac{p_{dC}}{N_k}.$$

Reasoning by induction on j, we get :

$$\mathbb{P}\big(B_1 \cap \cdots \cap B_j\big) = \Big(1 - \frac{p_{dC}}{N_k}\Big)^j, \quad 1 \leq j \leq N_k. \tag{5.3}$$

Since $\overline{D_k(C)} = B_1 \cap \cdots \cap B_{N_k}$, then (5.1) follows. Inequality (5.2) is a consequence of

$$1 - \alpha x \leq (1-x)^\alpha \leq 1 - \alpha x + \frac{\alpha(\alpha-1)}{2}x^2, \quad 0 \leq x \leq 1,\ \alpha \geq 1. \tag{5.4}$$

■

Remark 5.2 *For a F cell, it is enough to change p_{dC} into p_{dF} and $D_k(C)$ into $D_k(F)$ in the identities* (5.1) *and* (5.2).

The estimate provided by Lemma 5.1 will be used twice, in the proofs of Lemma 5.3 and Proposition 3.4 (see Section 5.3).
Consider a C cell which is born at time step $k_0 - 1$ and which starts to be active at time step k_0. Let $T(C)$ be the lifetime of this cell, it is the first integer $k \geq 1$ such that the C cell dies at the time step $k_0 - 1 + k$. By definition $T(C) \geq 1$. The distribution of this variable is unknown. However, thanks to (5.2), we can give an approximation of its distribution function.

Lemma 5.3 *For any integer $k \geq 0$,*

$$(1 - p_{dC})^k \leq \mathbb{P}_{\nu_0}\big(T(C) > k\big) \leq \Big(1 - p_{dC} + \frac{p_{dC}^2}{2}\Big)^k \tag{5.5}$$

Proof. Set $n = k_0 - 1 + k$, then

$$\mathbb{P}^{|n}_{\nu_0}\big(T(C) > k+1\big) = 1_{\{T(C)>k\}}\Big(1 - \mathbb{P}^{|n}_{\nu_0}\big(D_n(C)\big)\Big), \quad k \geq 0.$$

We take the expectation, using (5.2) we get :

$$(1-p_{dC})\mathbb{P}_{\nu_0}\big(T(C) > k\big) \leq \mathbb{P}_{\nu_0}\big(T(C) > k+1\big) \leq \Big(1 - p_{dC} + \frac{p^2_{dC}}{2}\Big)\mathbb{P}_{\nu_0}\big(T(C) > k\big).$$

The double inequality (5.5) is obtained by reasoning by recurrence on the integer k. ∎

Recall that the median of a random variable Y with integer values is its quantile of order $1/2$:

$$q_{1/2}(Y) = \max\Big\{k \geq 1,\ \mathbb{P}(Y \leq k) \leq \frac{1}{2}\Big\}.$$

Lemma 5.4 *Let $0 < a \leq b < 1$, and Y be a random variable which takes its values in $\{1, 2, \cdots\}$ and such that :*

$$(1-b)^k \leq \mathbb{P}(Y > k) \leq (1-a)^k, \quad \forall\, k \geq 0. \tag{5.6}$$

Then

$$\Big\lfloor \frac{\ln 2}{\ln(1/(1-b))} \Big\rfloor \leq q_{1/2}(Y) \leq \Big\lfloor \frac{\ln 2}{\ln(1/(1-a))} \Big\rfloor. \tag{5.7}$$

Proof. For any $0 < \rho < 1$, we have :

$$n \geq \Big\lfloor \frac{\ln 2}{\ln(1/\rho)} \Big\rfloor + 1 \ \Leftrightarrow\ \rho^n < \frac{1}{2}. \tag{5.8}$$

We take $\rho = 1 - a$ and $k = \Big\lfloor \frac{\ln 2}{\ln(1/\rho)} \Big\rfloor + 1$. Relations (5.6) and (5.8) imply

$$1 - \mathbb{P}(Y \leq k) = \mathbb{P}(Y > k) \leq \rho^k < \frac{1}{2} \ \Rightarrow\ \mathbb{P}(Y \leq k) > \frac{1}{2} \ \Rightarrow\ q_{1/2}(Y) < k.$$

Similarly, with $\rho = 1 - b$ et $k = \Big\lfloor \frac{\ln 2}{\ln(1/\rho)} \Big\rfloor$ we get :

$$1 - \mathbb{P}(Y \leq k) = \mathbb{P}(Y > k) \geq \rho^k \geq \frac{1}{2} \ \Rightarrow\ \mathbb{P}(Y \leq k) \leq \frac{1}{2} \ \Rightarrow\ k \leq q_{1/2}(Y).$$

∎

We now have all the elements to prove Proposition 3.1. We consider the relation (3.1) which only concerns the C cells. A direct use of inequalities (5.5) and (5.7) leads to : $q_- \leq q_{1/2}\big(T(C)\big) \leq q_+$, where :

$$q_- = \Big\lfloor \frac{\ln 2}{\ln\big\{1/(1-p_{dC})\big\}} \Big\rfloor, \quad q_+ = \Big\lfloor \frac{\ln 2}{\ln\Big\{1/\big(1 - p_{dC} + \frac{p^2_{dC}}{2}\big)\Big\}} \Big\rfloor.$$

By an easy calculation, we have :

$$q_+ - q_- \leq 1 + \frac{\ln 2}{\ln\Big(1 - p_{dC} + \frac{p^2_{dC}}{2}\Big)\ \ln(1-p_{dC})} \ln\Big(1 + \frac{p^2_{dC}}{2(1-p_{dC})}\Big).$$

To obtain (3.1), it is enough to use $\ln(1+x) < x$, for any $x > -1$.

5.2 Proof of Proposition 3.2

If the F cell is never completely surrounded during time step $k+1$, then $Z_k(moveF) = Z'_k(moveF)$. Otherwise, let us note $i_1, \cdots, i_r$ the sub-periods when the F cell is fully surrounded where $r = \Gamma_k(F)$. Note that $Z_k(moveF) = Z'_k(moveF)$ means that there is no virtual move. Moreover the probability that a virtual shift occurs at time i_j is $\frac{1}{N_k}(1-p_{dF})\frac{\alpha}{5}$. Consequently

$$\mathbb{P}^{|k}_{\nu_0}\Big(Z_k(moveF) = Z'_k(moveF)\big|i_1, \cdots, i_r\Big) = \Big(1 - \frac{1}{N_k}(1-p_{dF})\frac{\alpha}{5}\Big)^{\Gamma_k(F)}.$$

Using (5.4) we have :

$$\mathbb{P}^{|k}_{\nu_0}\big(Z_k(moveF) < Z'_k(moveF)\big) \leq \frac{1}{N_k}(1-p_{dF})\frac{\alpha}{5}\,\mathbb{E}^{|k}_{\nu_0}\big(\Gamma_k(F)\big) \leq \frac{1}{N_k}\mathbb{E}^{|k}_{\nu_0}\big(\Gamma_k(F)\big).$$

5.3 Proof of Proposition 3.4

We start with a lemma which will also be used in the proof of Proposition 3.6.

Lemma 5.5 *Let $0 < \lambda < a < 1$, $\lambda_0 \geq 0$ and $b > 0$. We suppose that the two sequences of real numbers $(x_n)_{n\geq 0}$ and $(y_n)_{n\geq 1}$ satisfy*

$$x_{n+1} = (1-a)x_n + b + y_{n+1}, \quad n \geq 0 \tag{5.9}$$

with $x_0 \geq 0$ and

$$0 \leq y_{n+1} \leq \lambda_0 + \lambda x_n, \quad n \geq 0. \tag{5.10}$$

Then

$$x_n = \frac{b}{a}\big(1-(1-a)^n\big) + (1-a)^n x_0 + \epsilon_n, \quad n \geq 0 \tag{5.11}$$

where $\epsilon_0 = 0$ and for any $n \geq 1$,

$$0 \leq \epsilon_n \leq \frac{1}{a}\big(1-(1-a)^n\big)\left(\lambda_0 + \lambda\Big(\frac{b+\lambda_0}{a-\lambda} + x_0\Big)\right) \tag{5.12}$$

$$\leq \frac{1}{a}\left(\lambda_0 + \lambda\Big(\frac{b+\lambda_0}{a-\lambda} + x_0\Big)\right). \tag{5.13}$$

Proof. We deduce from (5.9) and (5.10) :

$$x_{n+1} \leq (1-a+\lambda)x_n + b + \lambda_0, \quad n \geq 0.$$

Note that $0 < 1-a+\lambda < 1$. A direct induction reasoning allows to show

$$0 \leq x_n \leq \frac{b+\lambda_0}{a-\lambda} + x_0, \quad n \geq 0. \tag{5.14}$$

We suppose that (5.11) occurs and show that this equality is verified when n is changed into $n+1$. Using both (5.9) and (5.10) we obtain :

$$x_{n+1} = \frac{b}{a}\big(1-(1-a)^{n+1}\big) + (1-a)^{n+1}x_0 + \epsilon_{n+1}$$

where $\epsilon_{n+1} = y_{n+1} + (1-a)\epsilon_n$. We set $\epsilon_0 = 0$, a reasoning by recurrence allows to show

$$\epsilon_{n+1} = (1-a)^{n+1}\Big(\sum_{k=0}^{n} \frac{y_{k+1}}{(1-a)^{k+1}}\Big), \quad n \geq 1.$$

Relations (5.10) and (5.14) imply :

$$\epsilon_{n+1} \leq \lambda_0\Big[\frac{1}{a}\big(1-(1-a)^{n+1}\big)\Big] + \lambda\Big[\Big(\frac{b+\lambda_0}{a-\lambda} + x_0\Big) \times \frac{1}{a}\big(1-(1-a)^{n+1}\big)\Big].$$

This shows (5.12) where n is changed into $n+1$. ■

We only prove(3.16). According to the definition of the streamlined model :

$$\mathbb{E}_{\nu_0}^{|k}\big(N_{k+1}(F)\big) = N_k(F) + p_{istaF} - N_k(F)P_{\nu_0}^{|k}\big(D_k(F)\big).$$

We take the expectation on both sides, we get

$$\mathbb{E}_{\nu_0}\big(N_{k+1}(F)\big) = (1-p_{dF})\,\mathbb{E}_{\nu_0}\big(N_k(F)\big) + p_{istaF} + \theta_{k+1} \tag{5.15}$$

where $\theta_{k+1} = \mathbb{E}_{\nu_0}\Big[\Big(p_{dF} - P_{\nu_0}^{|k}\big(D_k(F)\big)\Big)N_k(F)\Big]$. According to Lemma 5.1 :

$$0 \leq \theta_{k+1} \leq \frac{p_{dF}^2}{2}\mathbb{E}_{\nu_0}\big(N_k(F)\big).$$

Then applying Lemma 5.5 with $x_k = \mathbb{E}_{\nu_0}\big(N_k(F)\big)$ leads to

$$\mathbb{E}_{\nu_0}\big(N_k(F)\big) = \Big(N_0(F) - \frac{p_{istaF}}{p_{dF}}\Big)(1-p_{dF})^k + \frac{p_{istaF}}{p_{dF}} + \epsilon_k \tag{5.16}$$

and $0 \leq \epsilon_k \leq \frac{p_{dF}}{2}\Big(\frac{p_{istaF}}{p_{dF}(1-p_{dF}/2)} + N_0(F)\Big)$.

5.4 Proof of Proposition 3.6

The proof of Proposition 3.6 is based on the two lemmas 5.6 and 5.7.

Lemma 5.6 *For any $0 \leq i \leq 19$:*

$$\begin{aligned}\mathbb{E}_{\nu_0}\big(N_{(i+1)T_y}(F)\big) \;=\; & (1-p_{dF})^{T_y}\,\mathbb{E}_{\nu_0}\big(N_{iT_y}(F)\big) + \frac{p_{istaF}}{p_{dF}}\big(1-(1-p_{dF})^{T_y}\big) \\ & + (1-p_{dF})^{T_y-1}N(iexaF)p_{iexaF} + \eta_{i+1}\end{aligned} \tag{5.17}$$

and

$$0 \leq \eta_{i+1} \leq \frac{p_{istaF}}{2(1-p_{dF}/2)} + \frac{p_{dF}}{2}\big(p_{istaF} + N(iexaF)p_{iexaF}\big) + \frac{p_{dF}(1+p_{dF})}{2}\,\mathbb{E}_{\nu_0}\big(N_{iT_y}(F)\big) \tag{5.18}$$

where one year equals $T_y = 175\,200$ time steps.

Proof. **1)** Let $0 \leq i \leq 19$. We start from (5.15) and (5.16) and apply Lemma 5.5 with $x_k = \mathbb{E}_{\nu_0}\big(N_k(F)\big)$ where $iT_y + 1 \leq k \leq (i+1)T_y$:

$$\mathbb{E}_{\nu_0}\big(N_{(i+1)T_y}(F)\big) = \frac{p_{istaF}}{p_{dF}}\big(1-(1-p_{dF})^{T_y-1}\big)+(1-p_{dF})^{T_y-1}\mathbb{E}_{\nu_0}\big(N_{iT_y+1}(F)\big)+\epsilon_{T_y-1} \quad (5.19)$$

where

$$0 \leq \epsilon_{T_y-1} \leq \frac{p_{dF}}{2}\Big(\frac{p_{istaF}}{p_{dF}(1-p_{dF}/2)} + \mathbb{E}_{\nu_0}\big(N^{COPD}_{iT_y+1}(F)\big)\Big). \quad (5.20)$$

We add $N(iexaF)$ F cells with probability p_{iexaF}, at the end of the time step iT_y, reasoning as in the proof of Proposition 3.4, we have :

$$\mathbb{E}_{\nu_0}\big(N_{iT_y+1}(F)\big) = (1-p_{dF})\,\mathbb{E}_{\nu_0}\big(N_{iT_y}(F)\big) + p_{istaF} + N(iexaF)p_{iexaF} + \theta_1 \quad (5.21)$$

where

$$0 \leq \theta_1 \leq \frac{(p_{dF})^2}{2}\mathbb{E}_{\nu_0}\big(N_{iT_y}(F)\big). \quad (5.22)$$

Synthesizing (5.19) and (5.21) we obtain (5.17) and $0 \leq \eta_{i+1} = (1-p_{dF})^{T_y-1}\theta_1 + \epsilon_{T_y-1} \leq \theta_1 + \epsilon_{T_y-1}$.
Using (5.20), (5.21) and (5.22) we obtain :

$$\epsilon_{T_y-1} \leq \frac{p_{istaF}}{2(1-p_{dF}/2)} + \epsilon^*$$

where

$$\begin{aligned}\epsilon^* &= \frac{p_{dF}}{2}\Big[(1-p_{dF})\,\mathbb{E}_{\nu_0}\big(N_{iT_y}(F)\big) + p_{istaF} + N(iexaF)p_{iexaF} + \theta_1\Big] \\ &\leq \frac{p_{dF}}{2}\Big[p_{istaF} + N(iexaF)p_{iexaF}\big) + \mathbb{E}_{\nu_0}\big(N_{iT_y}(F)\big)\Big].\end{aligned}$$

Then inequality (5.18) follows directly. ■

Lemma 5.7 *We have :*

$$\begin{aligned}\mathbb{E}_{\nu_0}\big(N_T(F)\big) &= \frac{p_{istaF}}{p_{dF}} + (1-p_{dF})^T\Big(N_0(F) - \frac{p_{istaF}}{p_{dF}}\Big) \\ &\quad + \frac{(1-p_{dF})^{T_y-1}}{1-(1-p_{dF})^{T_y}}\big(1-(1-p_{dF})^T\big)N(iexaF)p_{iexaF}\Big) + \epsilon'_{20}\end{aligned} \quad (5.23)$$

where $0 \leq \epsilon'_{20} \leq R'$ and R' has been defined by (3.22).

Proof. We apply Lemme 5.5 with $x_i = \mathbb{E}_{\nu_0}\big(N_{iT_y}(F)\big)$ and $0 \leq i \leq 20$:

$$\begin{aligned}\mathbb{E}_{\nu_0}\big(N_T(F)\big) &= (1-p_{dF})^T\Big(N_0(F) - \frac{p_{istaF}}{p_{dF}} - \frac{(1-p_{dF})^{T_y-1}}{1-(1-p_{dF})^{T_y}}N(iexaF)p_{iexaF}\Big) \\ &\quad + \frac{p_{istaF}}{p_{dF}} + \frac{(1-p_{dF})^{T_y-1}}{1-(1-p_{dF})^{T_y}}N(iexaF)p_{iexaF} + \varepsilon'_{20}\end{aligned}$$

This shows (5.23). Moreover $0 \leq \varepsilon'_{20} \leq R'$. ■

We apply (5.23) and (3.24), we easily obtain :

$$\mathbb{E}_{\nu_0}\big(N_T(F)\big) = 2N_0(F) + \varepsilon'_{20}.$$

This implies (3.25).

6 Annex

Table 1. Definition of the notations and parameters of the model

	Symbols	Meanings
Surface of interest	$\mathcal{L}$	Lamina propria (=peribronchial area)
	x_0	Side length of the units of the lattice $\mathcal{L}$
General	$M(s)$	Neighbourhood of the site s
	$V(s)$	Number of F and C cells belonging to $M(s)$
	$V(F)(s)$	Number of F cells belonging to $M(s)$
	$V(C)(s)$	Number of C cells belonging to $M(s)$
	$N_k(F)$	Number of F cells at the beginning of the time step k
	$N_k(C)$	Number of C cells at the beginning of the time step k
Cell death	p_{dF}	Probability for a F cell to die
	p_{dC}	Probability for a C cell to die
	p_{dC+}	Increased probability for a C cell to die
	σ	Threshold number of neighbouring C cells, above which the probability of dying is increased from p_{dC} to p_{dC+}
Cell proliferation	p_F	Probability for a F cell to divide
	p_C	Probability for a C cell to divide
	$p_{C/F}$	Increased probability for a C cell to divide
	λ	Threshold number of neighbouring C cells of an empty s' site belonging to $M(s)$, above which the considered C cell does not divide

Cell displacement	$P_F(s, s')$	Probability for a F cell to go from s to s'
	$P_C(s, s')$	Probability for a C cell to go from s to s'
	f_F	Function that is involved in the definition of $P_F(s, s')$ and which is applied to $V_C(F)(s')$ where s' is empty, $s' \neq s$ and $s' \in M(s)$
	f_C	Function that is involved in the definition of $P_C(s, s')$ and which is applied to $V(s')$ where s' is empty, $s' \neq s$ and $s' \in M(s)$
	ϵ_F	Value taken by f_F to reflect a low attraction
	ϵ_C	Value taken by f_C to reflect a low attraction
Cell infiltration	p_{istaF}	Probability for a F cell to get infiltrated at the beginning of a 3 minutes time step
	p_{istaC}	Probability for a C cell to get infiltrated at the beginning of a 3 minutes time step
	p_{iexaF}	Probability for a F cell to get infiltrated during an exacerbation
	p_{iexaC}	Probability for a C cell to get infiltrated during an exacerbation
	$N(iexaF)$	Number of F cell that are infiltrated during an exacerbation
	$N(iexaC)$	Number of C cell that are infiltrated during an exacerbation

Table 2. Numerical values of the streamlined model parameters depending in control and COPD situations

Symbols	x_0	$N_0(F)$	$N_0(C)$	p_{dF}^{ctl}	p_{dF}^{COPD}	p_{dC}^{ctl}	p_{dC}^{COPD}
Numerical values	$7\ \mu m$	19	118	4.8×10^{-6}	2.4×10^{-6}	10^{-4}	5×10^{-5}

Symbols	p_{dC+}^{ctl}	p_{dC+}^{COPD}	σ	p_F	p_C	$p_{C/F}^{ctl} = p_{C/F}^{COPD}$	λ	$\epsilon_F = \epsilon_C$
Numerical values	4×10^{-4}	2×10^{-4}	9	0	0	1.25×10^{-2}	0	10^{-3}

Symbols	p_{istaF}^{ctl}	p_{istaF}^{COPD}	p_{istaC}^{ctl}	p_{istaC}^{COPD}	p_{iexaF}^{ctl}	p_{iexaF}^{COPD}
Numerical values	9.12×10^{-5}	4.56×10^{-5}	1.18×10^{-2}	5.9×10^{-3}	0	9.93×10^{-1}

Symbols	p_{iexaC}^{ctl}=p_{iexaC}^{COPD}	$N(iexaF)^{ctl}$	$N(iexaF)^{COPD}$	$N(ixaC)$
Numerical values	0	0	10	0

References

[1] T. Afroj, A. Mitsuhashi, Ogino H., A. Saijo, K. Otsuka, H. Yoneda, M. Tobiume, N.T. Nguyen, H. Goto, K. Koyama, M. Sugimoto, O. Kondoh, H. Nokihara, and Y. Nishioka. Blockade of pd-1/pd-l1 pathway enhances the antigen-presenting capacity of fibrocytes. J. Immunol., 206(6) :1204–1214, 2021.

[2] M. C. Basil, F. L. Cardenas-Diaz, J. J. Kathiriya, M. P. Morley, J. Carl, A. N. Brumwell, J. Katzen, K. J. Slovik, A. Babu, S. Zhou, M. M. Kremp, K. B. McCauley, S. Li, J. D. Planer, S. S. Hussain, X. Liu, R. Windmueller, Y. Ying, K. M. Stewart, M. Oyster, and E. E. Morrisey. Human distal airways contain a multipotent secretory cell that can regenerate alveoli. Nature, 604(7904) :120–126, 2022.

[3] L. Benítez, L. Barberis, and C.A. Condat. Modeling tumorspheres reveals cancer stem cell niche building and plasticity. Physica A : Statistical Mechanics and its Applications, 533 :121906, 2019.

[4] Y. W. Chen, J. M. Leung, and D. D. Sin. A Systematic Review of Diagnostic Biomarkers of COPD Exacerbation. PLoS One, 11(7) :e0158843, 2016.

[5] A. Deutsch and S. Dormann. Cellular automaton modeling of biological pattern formation. Modeling and Simulation in Science, Engineering and Technology. Birkhäuser/Springer, New York, 2017. Characterization, examples, and analysis, Second edition.

[6] I. Dupin, B. Allard, A. Ozier, E. Maurat, O. Ousova, E. Delbrel, T. Trian, H.-N. Bui, C. Dromer, O. Guisset, E. Blanchard, G. Hilbert, F. Vargas, M. Thumerel, R. Marthan, P.-O. Girodet, and P. Berger. Blood fibrocytes are recruited during acute exacerbations of chronic obstructive pulmonary disease through a cxcr4-dependent pathway. J. Allergy Clin. Immunol., 137 :1036–1042, 2016.

[7] I. Dupin, M. Thumerel, E. Maurat, F. Coste, E. Eyraud, H. Begueret, T. Trian, M. Montaudon, R. Marthan, P.-O. Girodet, and P. Berger. Fibrocyte accumulation in the airway walls of copd patients. Eur. Respir. J., 54, 2019.

[8] K. H. Ely, T. Cookenham, A. D. Roberts, and D. L. Woodland. Memory T cell populations in the lung airways are maintained by continual recruitment. J Immunol, 176(1) :537–543, Jan 2006.

[9] C. M. Freeman, C. H. Martinez, J. C. Todt, F. J. Martinez, M. K. Han, D. L. Thompson, L. McCloskey, and J. L. Curtis. differentiation factor-15 (GDF-15) in peripheral blood. Respir Res, 16 :94, Aug 2015.

[10] S. Ghosh and S. Bhattacharya. Computational model on covid-19 pandemic using probabilistic cellular automata. SN Computer Science, 2021.

[11] D.A. Groneberg and Chung K.F. Models of chronic obstructive pulmonary disease. Respir Res., 5(1) :18, 2004.

[12] E. J. Hackett-Jones, K. A. Landman, D. F. Newgreen, and D. Zhang. On the role of differential adhesion in gangliogenesis in the enteric nervous system. J. Theor. Biol., 287 :148–159, 2011.

[13] O. Häggström. Finite Markov chains and algorithmic applications, volume 52 of London Mathematical Society Student Texts. Cambridge University Press, Cambridge, 2002.

[14] N. L. Harris, V. Watt, F. Ronchese, and G. Le Gros. Differential T cell function and fate in lymph node and nonlymphoid tissues. J Exp Med, 195(3) :317–326, Feb 2002.

[15] M. Hasegawa, Y. Nasuhara, Y. Onodera, H. Makita, K. Nagai, S. Fuke, Y. Ito, T. Betsuyaku, and M. Nishimura. Airflow limitation and airway dimensions in chronic obstructive pulmonary disease. Am. J. Respir. Crit. Care Med., 173 :1309–1315, 2006.

[16] H. Hatzikirou, L. Brusch, C. Schaller, M. Simon, and A. Deutsch. Prediction of traveling front behavior in a lattice-gas cellular automaton model for tumor invasion. Comput. Math. Appl., 59(7) :2326–2339, 2010.

[17] H. D. Hickman, G. V. Reynoso, B. F. Ngudiankama, S. S. Cush, J. Gibbs, J. R. Bennink, and J. W. Yewdell. CXCR3 chemokine receptor enables local CD8(+) T cell migration for the destruction of virus-infected cells. Immunity, 42(3) :524–537, Mar 2015.

[18] R.J. Hogan, L.S. Cauley, K.H. Ely, T. Cookenham, A.D. Roberts, J.W. Brennan, S. Monard, and D.L. Woodland. Long-term maintenance of virus-specific effector memory cd8+ t cells in the lung airways depends on proliferation. J. Immunol., 169 :4976–4981, 2002.

[19] P. Hogeweg. Cellular automata as a paradigm for ecological modeling. Appl. Math. Comput., 27(1) :81–100, 1988.

[20] J.C. Hogg, F. Chu, S. Utokaparch, R. Woods, W.M. Elliott, L. Buzatu, R.M. Cherniack, R.M. Rogers, F.C. Sciurba, H.O. Coxson, and P.D. Paré. The nature of small-airway obstruction in chronic obstructive pulmonary disease. N. Engl. J. Med., 350 :2645–2653, 2004.

[21] J. R. Hurst, J. Vestbo, A. Anzueto, N. Locantore, H. Müllerova, R. Tal-Singer, B. Miller, D. A. Lomas, A. Agusti, W. Macnee, P. Calverley, S. Rennard, E. F. Wouters, J. A. Wedzicha, H. Coxson, L. Edwards, R. Tal-Singer, D. Lomas, W. MacNee, E. Silverman, C. Crim, J. Vestbo, J. Yates, A. Agusti, P. Calverley, B. Celli, C. Crim, B. Miller, W. MacNee, S. Rennard, R. Tal-Singer, E. Wouters, J. Yates, Y. Ivanov, K. Kostov, J. Bourbeau, M. Fitzgerald, P. Hernandez, K. Killian, R. Levy, F. Maltais, D. O'Donnell, J. Krepelka, J. Vestbo, E. Wouters, D. Quinn, P. Bakke, M. Kosnik, A. Agusti, J. Sauleda, Y. Feschenko, V. Gavrisyuk, L. Yashina, N. Monogarova, P. Calverley, D. Lomas, W. MacNee, D. Singh, J. Wedzicha, A. Anzueto, S. Braman, R. Casaburi, B. Celli, G. Giessel, M. Gotfried, G. Greenwald, N. Hanania, D. Mahler, B. Make, S. Rennard, C. Rochester, P. Scanlon, D. Schuller, F. Sciurba, A. Sharafkhaneh, T. Siler, E. Silverman, A. Wanner, R. Wise, and R. ZuWallack. Susceptibility to exacerbation in chronic obstructive pulmonary disease. N Engl J Med, 363(12) :1128–1138, Sep 2010.

[22] M. Karakioulaki, E. Papakonstantinou, and D. Stolz. Extracellular matrix remodelling in COPD. Eur Respir Rev, 29(158), Dec 2020.

[23] D.I. Krimmer and B. G. Oliver. What can in vitro models of copd tell us ? Pulmonary pharmacology & therapeutics, 24(5) :471–477, 2011.

[24] R. L. Kusko, J. F. Brothers, J. Tedrow, K. Pandit, C. Huleihel, L.and Perdomo, B.and Kass D. Liu, G.and Juan-Guardela, M.and Martinez F. Zhang, S.and Lenburg, J. Quackenbush, A.and Geraci M. Sciurba, F.and Limper, Yang, D. A. I., Schwartz, A. Beane, J.and Spira, and N. Kaminski. Integrated genomics reveals convergent transcriptomic networks underlying chronic obstructive pulmonary disease and idiopathic pulmonary fibrosis. American journal of respiratory and critical care medicine, 194(8) :948–960, 2016.

[25] K. A. Landman and D. F. Newgreen. PCA modelling of multi-species cell clusters : ganglion development in the gastrointestinal nervous system. In Probabilistic cellular automata, volume 27 of Emerg. Complex. Comput., pages 261–277. Springer, Cham, 2018.

[26] C. Launay, B. Galerne, and A. Desolneux. Exact sampling of determinantal point processes without eigendecomposition. J. Appl. Probab., 57(4) :1198–1221, 2020.

[27] C.W. Lawrence and T.J. Braciale. Activation, differentiation, and migration of naive virus-specific cd8+ t cells during pulmonary influenza virus infection. J. Immunol., 173 :1209–1218, 2004.

[28] D. Lehotzky, R. Sipahi, and G. Zupanc. Cellular automata modeling suggests symmetric stem-cell division, cell death, and cell drift as key mechanisms driving adult spinal cord growth in teleost fish. Journal of Theoretical Biology, 509 :22, 2021.

[29] C. Ling, K. Nishimoto, Z. Rolfs, L. M. Smith, B. L. Frey, and N. V. Welham. Differentiated fibrocytes assume a functional mesenchymal phenotype with regenerative potential. Sci Adv, 5(5) :eaav7384, 05 2019.

[30] P.-Y. Louis and F. R. Nardi, editors. Probabilistic cellular automata. Theory, applications and future perspectives, volume 27. Springer, 2018.

[31] A. Løkke, P. Lange, H. Scharling, P. Fabricius, and J. Vestbo. Developing COPD : a 25 year follow up study of the general population. Thorax, 61(11) :935–939, Nov 2006.

[32] H. Mahmoud and A. Chulahwat. A probabilistic cellular automata framework for assessing the impact of wui fires on communities. Procedia Engineering, 198 :1111–1122, 2017.

[33] L. Manukyan, S. A. Montandon, A. Fofonjka, S. Smirnov, and M. C. Milinkovitch. A living mesoscopic cellular automaton made of skin scales. Nature, 544(7649) :173–179, 04 2017.

[34] S.R. McMaster, J.J. Wilson, H. Wang, and J.E. Kohlmeier. Airway-resident memory cd8 t cells provide antigen-specific protection against respiratory virus challenge through rapid ifn-production. J. Immunol., 195 :203–209, 2015.

[35] P. Mrass, S.R. Oruganti, G.M. Fricke, J. Tafoya, J.R. Byrum, L. Yang, S.L. Hamilton, M.J. Miller, M.E. Moses, and J.L. Cannon. Rock regulates the intermittent mode of interstitial t cell migration in inflamed lungs. Nat. Commun., 2017.

[36] J. M. Nava-Sedeño, H. Hatzikirou, F. Peruani, and A. Deutsch. Extracting cellular automaton rules from physical Langevin equation models for single and collective cell migration. J. Math. Biol., 75(5) :1075–1100, 2017.

[37] T. C. O'Shaughnessy, T. W. Ansari, N. C. Barnes, and P. K. Jeffery. Inflammation in bronchial biopsies of subjects with chronic bronchitis : inverse relationship of cd8+ t lymphocytes with fev1. American journal of respiratory and critical care medicine, 155(3) :852–857, 1997.

[38] F. Peruani, A. Deutsch, and M. Bär. A mean-field theory for self-propelled particles interacting by velocity alignment mechanisms. The European Physical Journal Special Topics, 157 :111–122, 2008.

[39] J. J. Pothen, M. E. Poynter, and J. H. Bates. The inflammatory twitch as a general strategy for controlling the host response. Journal of Immunology (Baltimore, Md. : 1950), 190(7) :3510–3516, 2013.

[40] J. J. Pothen, M. E. Poynter, and J. H. Bates. A computational model of unresolved allergic inflammation in chronic asthma. American Journal of Physiology. Lung Cellular and Molecular Physiology, 308(4) :384–390, 2015.

[41] J. G. Propp and D. B. Wilson. Exact sampling with coupled Markov chains and applications to statistical mechanics. In Proceedings of the Seventh International Conference on Random Structures and Algorithms (Atlanta, GA, 1995), volume 9, pages 223–252, 1996.

[42] M. Puljic and R. Kozma. Narrow-band oscillations in probabilistic cellular automata. Phys. Rev. E, 78 :026214, Aug 2008.

[43] M. Saetta, A. Di Stephano, G. Turato, F.M. Facchini, L. Corbino, C.E. Mapp, P. Maestrelli, A. Ciaccia, and L.M. Fabbri. Cd8+ t-lymphocytes in peripheral airways of smokers with chronic obstructive pulmonary disease. Am. J. Respir. Crit. Care Med., 157 :822–826, 1998.

[44] R. Saunders, H. Kaul, R. Berair, S. Gonem, A. Singapuri, A. J. Sutcliffe, L. Chachi, M. S. Biddle, D. Kaur, M. Bourne, I. D. Pavord, A. J. Wardlaw, S. H. Siddiqui, R. A. Kay, B. S. Brook, R. H. Smallwood, and C. E. Brightling. Antagonism reduces airway smooth muscle mass in asthma by decreasing eosinophilia and myofibroblast recruitment. Sci Transl Med, 11(479), 02 2019.

[45] P. Scheipers and H. Reiser. Fas-independent death of activated cd4+ t lymphocytes induced by ctla-4 crosslinking. Proc. Natl. Acad. Sci., 95 :10083–10088, 1998.

[46] M. Schmidt, G. Sun, M. A. Stacey, L. Mori, and S. Mattoli. Identification of circulating fibrocytes as precursors of bronchial myofibroblasts in asthma. J Immunol, 171(1) :380–389, Jul 2003.

[47] J. Schyns, Q. Bai, C. Ruscitti, C. Radermecker, S. De Schepper, S. Chakarov, F. Farnir, D. Pirottin, F. Ginhoux, G. Boeckxstaens, F. Bureau, and T. Marichal. Non-classical tissue monocytes and two functionally distinct populations of interstitial macrophages populate the mouse lung. Nat. Commun., 10, 2019.

[48] A. N. Shiryayev. Probability, volume 95 of Graduate Texts in Mathematics. Springer-Verlag, New York, 1984. Translated from the Russian by R. P. Boas.

[49] L. Siena, M. Gjomarkaj, J. Elliot, E. Pace, A. Bruno, S. Baraldo, M. Saetta, M.R. Bonsignore, and A. Jame. Reduced apoptosis of cd8+ t-lymphocytes in the airways of smokers with mild/moderate copd. Respir. Med., 105 :1491–1500, 2011.

[50] H.S. Silva and M.L. Martins. A cellular automata model for cell differentiation. Physica A : Statistical Mechanics and its Applications, 322 :555–566, 2003.

[51] S. Takamura, H. Yagi, Y. Hakata, C. Motozono, S. R. McMaster, T. Masumoto, M. Fujisawa, T. Chikaishi, J. Komeda, J. Itoh, M. Umemura, A. Kyusai, M. Tomura, T. Nakayama, D. L. Woodland, J. E. Kohlmeier, and M. Miyazawa. Specific niches for lung-resident memory CD8+ T cells at the site of tissue regeneration enable CD69-independent maintenance. J Exp Med, 213(13) :3057–3073, 12 2016.

[52] A. van Haarst, L. McGarvey, and S Paglialunga. Review of drug development guidance to treat chronic obstructive pulmonary disease : Us and eu perspectives. Clinical pharmacology and therapeutics, 106(6) :1222–1235, 2019.

[53] Tamás Vicsek, András Czirók, Eshel Ben-Jacob, Inon Cohen, and Ofer Shochet. Novel type of phase transition in a system of self-driven particles. Phys. Rev. Lett., 75 :1226–1229, Aug 1995.

[54] H. Yoon, T.S. Kim, and T.J. Braciale. The cell cycle time of cd8+ t cells responding in vivo is controlled by the type of antigenic stimulus. PLoS ONE, 5, 2010.

[55] S. Zenke, M.M. Palm, J. Braun, A. Gavrilov, P. Meiser, J.P. J.P. Böttcher, N. Beyersdorf, S. Ehl, A. Gerard, T. Lämmermann, T.N. Schumacher, J.B. Beltman, and J.C. Rohr. Quorum regulation via nested antagonistic feedback circuits mediated by the receptors cd28 and ctla-4 confers robustness to t cell population dynamics. Immunity, 52 :313–327, 2020.